Journal of Medicinal Chemistry

Article

The Magic of Crystal Structure-Based Inhibitor Optimization: Development of a Butyrylcholinesterase Inhibitor with Picomolar Affinity and In Vivo Activity

Urban Košak, Boris Brus, Damijan Knez, Simon Žakelj, Jurij Trontelj, Anja Pišlar, Roman Šink, Marko Juki#, Marko Živin, Adrian Podkowa, Florian Nachon, Xavier Brazzolotto, Jure Stojan, Janko Kos, Nicolas Coquelle, Kinga Salat, Jacques-Philippe Colletier, and Stanislav Gobec

J. Med. Chem., **Just Accepted Manuscript** • DOI: 10.1021/acs.jmedchem.7b01086 • Publication Date (Web): 11 Dec 2017

ACS Publications

Journal of Medicinal Chemistry is published by the American Chemical Society. 1155 Sixteenth Street N.W., Washington, DC 20036

The Magic of Crystal Structure-Based Inhibitor Optimization: Development of a Butyrylcholinesterase Inhibitor with Picomolar Affinity and *In Vivo* Activity

Urban Košak,[‡] Boris Brus,[‡] Damijan Knez,[‡] Simon Žakelj,[‡] Jurij Trontelj,[‡] Anja Pišlar,[‡] Roman Šink,[‡] Marko Jukič,[‡] Marko Živin,[▲] Adrian Podkowa,[Δ] Florian Nachon,[ø] Xavier Brazzolotto,[ø] Jure Stojan,[■] Janko Kos,[‡] Nicolas Coquelle,[§] Kinga Sałat,[Δ] Jacques-Philippe Colletier[§] and Stanislav Gobec[‡,*]

[‡]Faculty of Pharmacy, University of Ljubljana, Aškerčeva 7, 1000 Ljubljana, Slovenia

[▲]Institute of Pathological Physiology, Faculty of Medicine, University of Ljubljana, Vrazov trg 2, 1000 Ljubljana, Slovenia

[ø] Institut de Recherche Biomédicale des Armées, 91223 Brétigny sur Orge, France

[Δ] Faculty of Pharmacy, Jagiellonian University, Medyczna 9 St., 30-688 Krakow, Poland

[■]Institute of Biochemistry, Faculty of Medicine, University of Ljubljana, Vrazov trg 2, 1000 Ljubljana, Slovenia

[§]University Grenoble Alpes, and CNRS and CEA, IBS, F-38044 Grenoble, France

Abstract

The enzymatic activity of butyrylcholinesterase (BChE) in the brain increases with the progression of Alzheimer's disease, thus classifying BChE as a promising drug target in advanced Alzheimer's disease. We used structure-based drug-discovery approaches to develop potent, selective and reversible human BChE inhibitors. The most potent, compound **3**, had a picomolar inhibition constant *versus* BChE due to strong cation-π interactions, as revealed by the solved crystal structure of its complex with human BChE. Additionally, compound **3** inhibits BChE *ex vivo*, and is non-cytotoxic. *In vitro* pharmacokinetic experiments show that compound **3** is highly protein bound, highly permeable, and metabolically stable. Finally, compound **3** crosses the blood-brain barrier, and it improves memory, cognitive functions, and learning abilities of mice in a scopolamine model of dementia. Compound **3** is thus a promising advanced lead compound for the development of drugs for alleviating symptoms of cholinergic hypofunction in patients with advanced Alzheimer's disease.

Introduction

Alzheimer's disease (AD) is a severe and irreversible progressive neurodegenerative disorder of the central nervous system.[1] Given the aging population in Western countries, the number of people who suffer from AD is expected to escalate in coming years, with AD prevalence predicted to reach over 100 million by the year 2050.[2] AD is characterized by gradual deterioration of cognitive abilities, accompanied by behavior that eventually interferes with the customary activities of daily living. Hallmarks of AD include aggregation and deposition of the protein tau[3] and amyloid-β (Aβ),[4,5] oxidative stress,[6] and death of cholinergic neurons in the basal forebrain. This results in reduced levels of the neurotransmitter acetylcholine (ACh) in the cerebral cortex and other brain areas. Taken together, severe memory and learning deficits are associated with AD.[7–9]

At the neuronal level, cholinergic neurotransmission is terminated by ACh hydrolysis through two types of cholinesterases (ChEs): acetylcholinesterase (AChE) and butyrylcholinesterase (BChE).[10] The AChE activity is dominant in the healthy brain (80%), where it catalyzes the hydrolysis of ACh to acetate and choline, while the BChE activity was initially considered to be non-essential for full functioning of the central nervous system.[11] Current treatments of patients with AD focus on drugs that can increase cholinergic neurotransmission by inhibiting the ChEs,[12] which include donepezil,[13] rivastigmine,[14] and the alkaloid galanthamine[15] (Figure 1A).

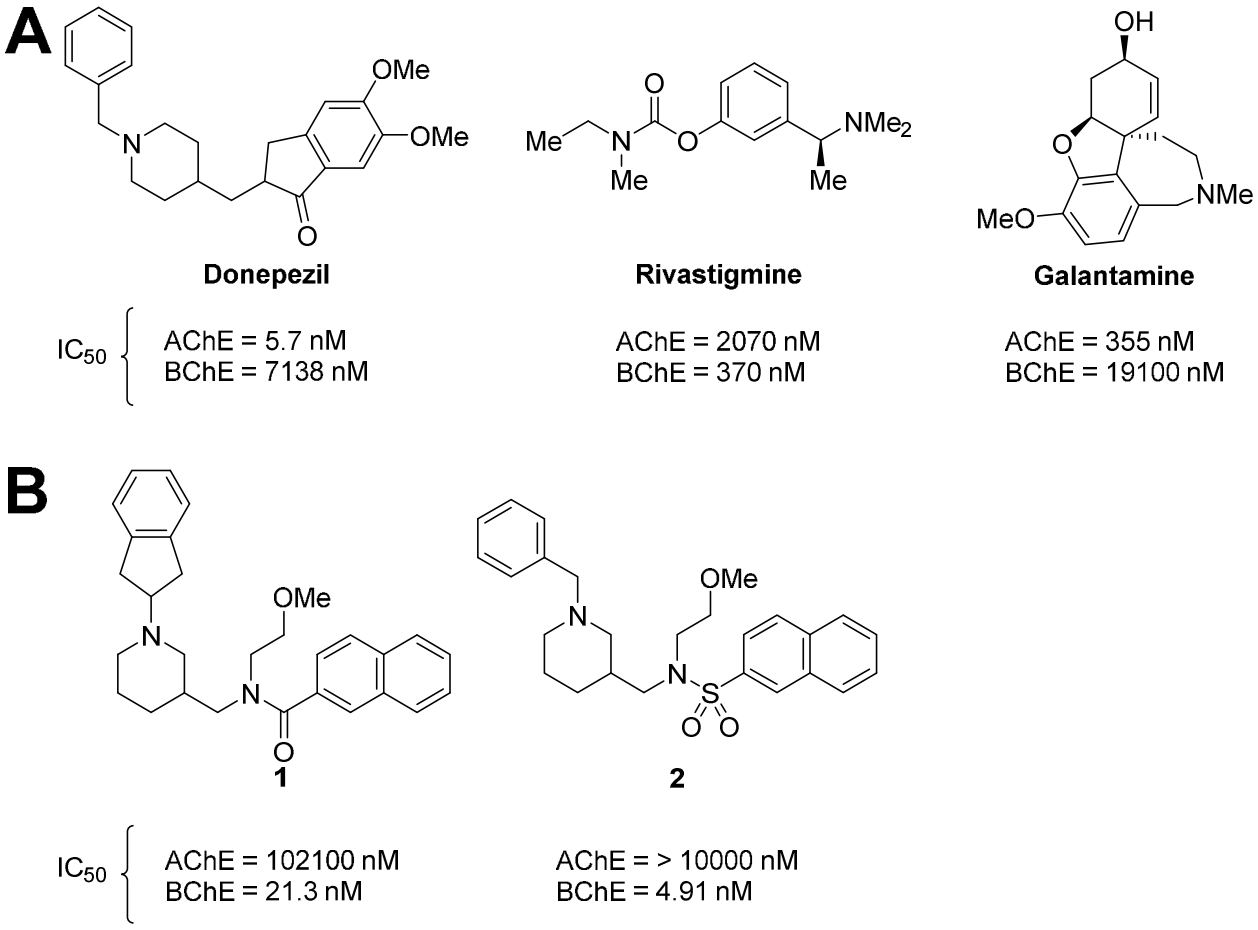

Figure 1. **Structures and IC_{50} values *versus* the cholinesterases.** (**A**) Donepezil, rivastigmine, and galantamine. (**B**) Selective BChE inhibitors, as hit compound **1** and sulfonamide **2**.

BChE activity is mainly associated with glial cells, as well as with vascular and neuronal structures, with BChE-positive neurons defined for the thalamus, neocortex, and amygdala.[16–18] As BChE can efficiently hydrolyze the ACh analog acetylthiocholine and can rescue cholinesterase function in the AChE nullizygote mouse, BChE might act as a co-regulator of the cholinergic activity in the central nervous system.[19–23] Indeed, the levels of BChE in certain parts of the brain show significant increases in the late stages of AD, with the ratio between BChE and AChE (BChE/AChE) increasing from 0.2 up to as much as 11.0 in certain parts of the brain; this

implies a shift from a supportive role to a leading role for BChE in the hydrolysis of the excess ACh.[24–27] Due to this altered BChE/AChE ratio and the demonstration of promising procognitive effects of BChE inhibition *in vivo* using selective BChE inhibitors,[28,29] targeting BChE has become a viable alternative for the treatment of patients with mild-to-late stages of AD.[28–31] Furthermore, the elevation of depleted ACh levels and the increase in the cognitive functions promoted by selective BChE inhibitors *in vivo* is not accompanied by the peripheral (parasympathomimetic) adverse effects[29,31] that are known to limit the use of AChE inhibitors.[32–34] Selective inhibition of brain BChE thus represents a useful strategy to ameliorate the cholinergic deficit and improve the cognitive performance of patients in the late stages of AD.

Using a hierarchical virtual screening protocol, we recently defined hit compound **1** (Figure 1B) as a potent, selective and reversible slow-tight–binding inhibitor of human BChE (huBChE).[35] We then used the structure of hit compound **1** to develop sulfonamide **2** (Figure 1B), which is the only *in vivo*–active noncovalent BChE inhibitor[29] among the large number of selective BChE inhibitors to have been reported.[28,29,36–41] However, the crystal structure of huBChE in complex with hit compound **1** (PDB ID 4TPK) revealed several additional opportunities for structural modifications of compound **1** to further improve its huBChE inhibitory potency.

Here, we report the design, synthesis and biochemical evaluation of a focused library of amide derivatives of hit compound **1**. The most potent of these, compound **3**, shows selective reversible huBChE inhibition in the picomolar concentration range. The crystal structure of its complex with the target enzyme (i.e., huBChE) reveals that two strong cation-π interactions are the basis of its greatly increased inhibitory potency. Additionally, compound **3** improves learning abilities, memory, and cognitive functions of mice in a model of the cholinergic deficit that characterizes AD, without producing any acute cholinergic adverse effects.

Results and Discussion

Design of the Inhibitors

Based on the chemical structure of hit compound **1**, **class I–VII** inhibitors were initially designed (Figure 2), with specific attention given to the production of inhibitors with drug-like properties.[42] The **class I** inhibitors were designed to investigate the importance of the naphthalene moiety of hit compound **1**. This moiety was replaced with other aromatic groups, including smaller substituted benzene rings, five- and six-membered heterocycles, and 6-substituted naphthalenes. Simultaneous modification of the naphthalene moiety and removal of the -$(CH_2)_2$OMe group from the amide nitrogen produced the **class II** inhibitors. In the **class III** inhibitors, the 2,3-dihydro-1*H*-inden moiety was replaced with a benzyl group, and the 2-naphthalene was either retained or replaced with modified naphthalenes. The **class IV** inhibitor was designed to examine the impact of simultaneous replacement of the 2,3-dihydro-1*H*-inden moiety with a benzyl group and of the removal of the -$(CH_2)_2$OMe group. Benzoxazole- or benzothiazole-containing compounds have been shown to bind to Aβ and to inhibit its aggregation.[43] Potential multifunctional compounds combining BChE inhibition and anti-Aβ aggregation properties were therefore designed here by replacing the 2,3-dihydro-1*H*-inden moiety of hit compound **1** with benzoxazole and benzothiazole in the **class V** inhibitors. To investigate the effects of the length of the *N*-alkyl chain attached to the amide nitrogen in compound **1**, compounds with an extended *N*-alkyl chain were also designed, as the **class VI** inhibitors. Finally, the **class VII** inhibitors are 1,4-disubstituted piperidines, which were designed to determine the influence of the piperidine ring disubstitution pattern (Figure 2).

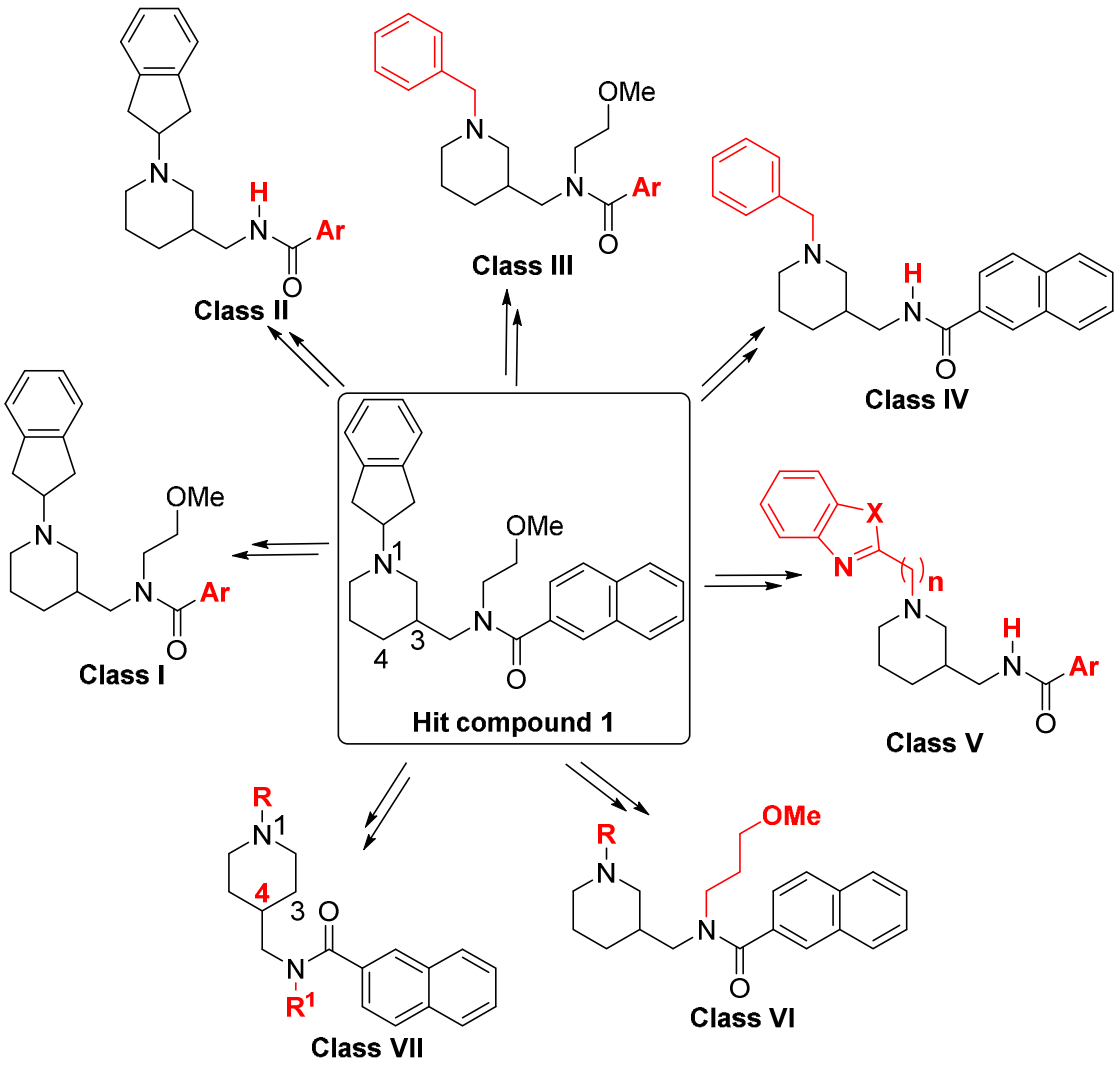

Figure 2. Design of the class I–VII inhibitors. The modifications introduced during each design step are indicated in red.

Compared to hit compound **1**, all of these **class I–VII** inhibitors were less potent huBChE inhibitors (Supporting Table S1). This thus called for rational structure-based drug design, which yielded the **class VIII** inhibitors (Figure 3). The crystal structure of the complex of compound **1** with huBChE (PDB ID 4TPK) had indeed revealed that the -$(CH_2)_2$OMe group of compound **1** is oriented toward the catalytic residues (i.e., Ser198, His438) and Trp82 in the choline-binding

pocket, although it did not appear to interact specifically with any of these residue (Figure 3A).[35] We hypothesized that the simple replacement of the -OMe group in compound **1** by -NMe_2 might improve the potency by contributing an additional cation-π interaction with Trp82. This Trp82 indeed stabilizes the natural substrate (and other ligands) through such interactions.[44] To enable these interactions with Trp82, the -NMe_2 group was used as the simplest basic center. However, compounds with an additional methylene group in the side chain [e.g., -$(CH_2)_3NMe_2$] were also designed (Figure 3B), to determine the optimal length between the amide nitrogen and the -NMe_2 group for optimal huBChE inhibition. Due to the limited size of the choline-binding pocket, further prolongation of the side chain did not appear reasonable.

Synthesis of the Inhibitors

The synthesis of **class VIII** inhibitors is shown in Figure 3. Nipecotic acid (**4**) was converted into benzoyl amide **5**,[45] which was then reacted with N^1,N^1-dimethylethane-1,2-diamine in the presence of TBTU to produce amide **6**. Compound **5** was also reacted with N^1,N^1-dimethylpropane-1,3-diamine in the presence of TBTU to produce amide **7**. $LiAlH_4$ was used to reduce both amide groups of compounds **6** and **7** and produce secondary amines **8** and **9**, which was reacted with 2-naphthoyl chloride to produce amides **10** and **11**. Secondary amines **8** and **9** were also converted into orthogonally protected piperidin-3-yl methanamines **12** and **13**, which were debenzylated to produce secondary amines **14** and **15**. This secondary amines was reacted with 1,3-dihydro-2*H*-inden-2-one in the presence of sodium triacetoxyborohydride [$NaBH(OAc)_3$] to produce tertiary amines **16** and **17**. TFA was used to remove the *tert*-butyloxycarbonyl protecting group from compounds **16** and **17** to provide amine tris(2,2,2-trifluoroacetates) **18** and **19**, which were then reacted with 2-naphthoyl chloride to produce

amides **3** and **20**. Compound **3** was converted into dichloride salt using 2 M solution of HCl in Et_2O.

Tert-butyl (2-hydroxyethyl)(methyl)carbamate (**21**) was converted into mesylate **22**, which then was used to alkylate amide **23** to produce compound **24**. Concentrated aqueous HCl in EtOH was used to remove the *tert*-butyloxycarbonyl protecting group from compound **24** to provide amide **25 dichloride**. Details of the synthesis of **class I-VII** inhibitors are given in Supporting Figures S1 to S7 and Supporting Discussion.

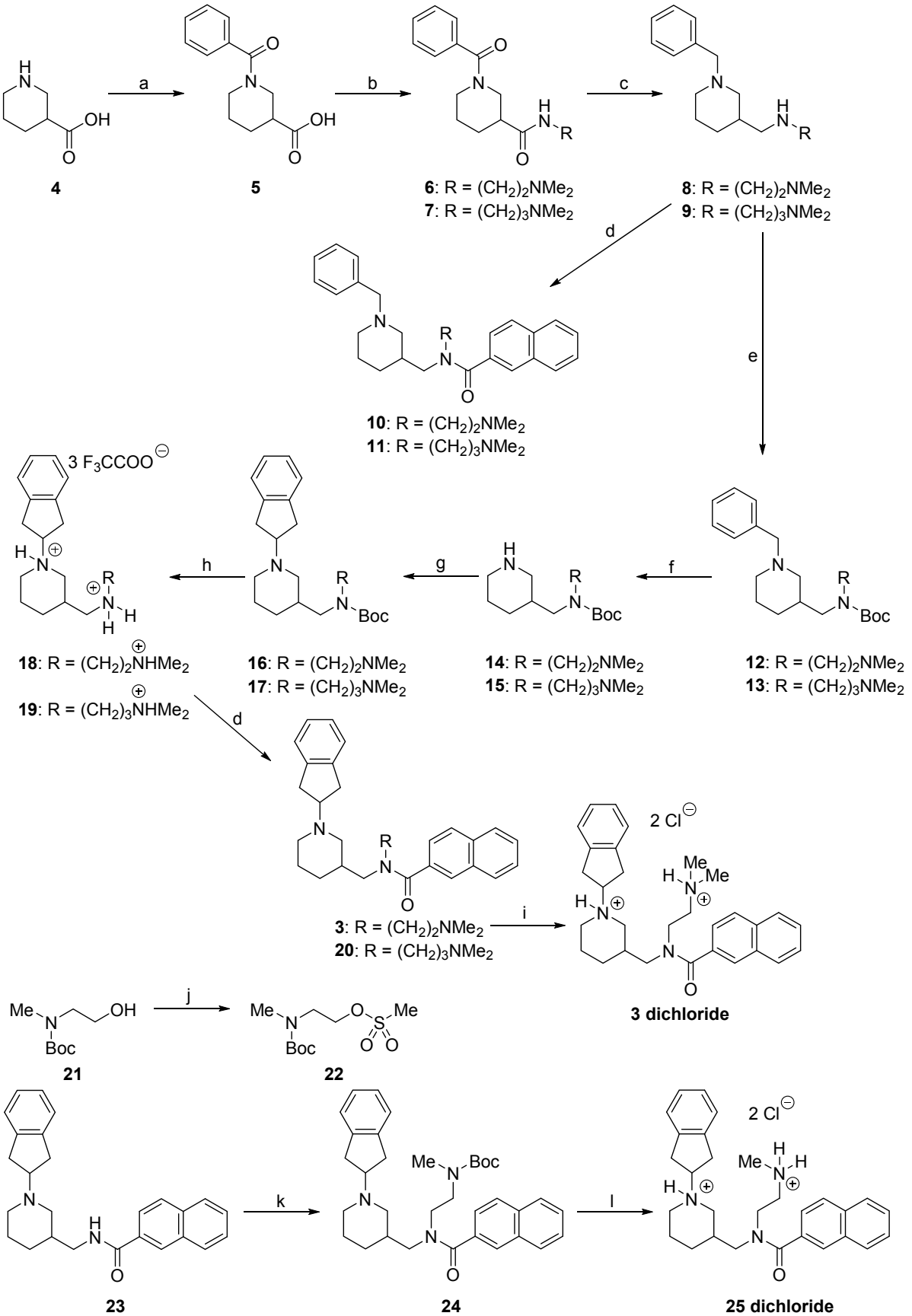
a
b
c
d
e
f
g
h
i
j
k
l
4
5
6: R = (CH2)2NMe2
7: R = (CH2)3NMe2
8: R = (CH2)2NMe2
9: R = (CH2)3NMe2
10: R = (CH2)2NMe2
11: R = (CH2)3NMe2
12: R = (CH2)2NMe2
13: R = (CH2)3NMe2
14: R = (CH2)2NMe2
15: R = (CH2)3NMe2
16: R = (CH2)2NMe2
17: R = (CH2)3NMe2
18: R = (CH2)2NHMe2
19: R = (CH2)3NHMe2
3 F3CCOO
3: R = (CH2)2NMe2
20: R = (CH2)3NMe2
2 Cl
3 dichloride
21
22
23
24
25 dichloride

Figure 3. Synthesis of class VIII inhibitors. Conditions and reagents: (**a**) (i) PhCOCl, K_2CO_3, THF–H_2O, 0 °C to rt, 22 h; (ii) 6 M HCl (aq), 0 °C (95%); (**b**) H_2N-$(CH_2)_n$-NMe2, TBTU, Et_3N, DCM, rt, 24 h (93% crude); (**c**) $LiAlH_4$, anhydrous THF, rt to reflux, under argon, 3.5 h (67%–78% crude); (**d**) 2-naphthoyl chloride, Et_3N, DCM, 0 °C to rt, 24 h (39%–85%); (**e**) Boc_2O, Et_3N, DCM, 0 °C to rt, 24 h (41%–55%); (**f**) cyclohexene, $Pd(OH)_2$/C cat., MeOH, rt to reflux, under argon, 24 h (98%–99% crude); (**g**) 1,3-dihydro-2*H*-inden-2-one, $NaBH(OAc)_3$, AcOH, 1,2-dichloroethane, under argon, 24 h (47%–69%); (**h**) TFA, DCM, rt, 24 h (95%–98%); (**i**) 2 M HCl solution in Et_2O, MeOH, under argon, 0 °C (15 min) to rt (90 min) (98%); (**j**) $MeSO_2Cl$, Et_3N, DCM, 0 °C to rt, 2 h (97% crude); (**k**) (i) NaH (60% dispersion), dry DMF, 0 °C to rt, 2 h; (ii) 88, rt to 50 °C, 72 h (51 %); (**l**) conc. aqueous HCl, EtOH, rt to 50 °C, 16 h (70%).

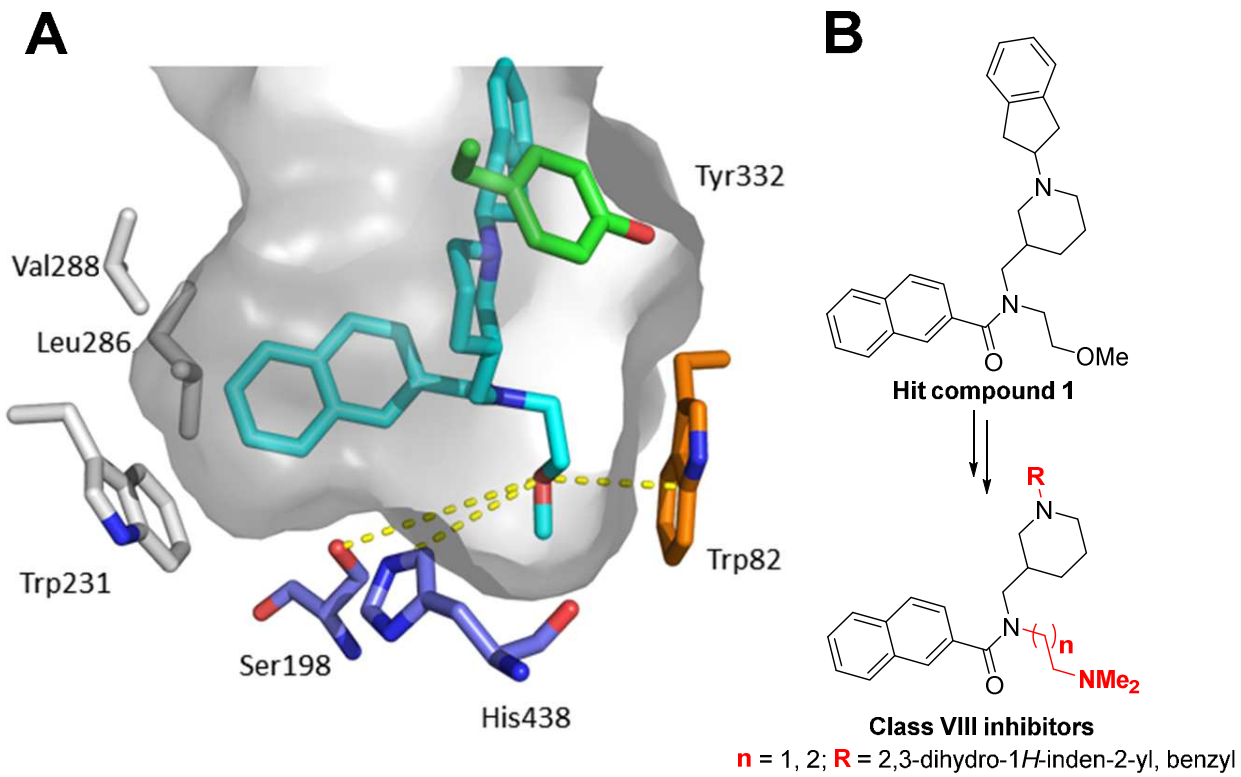

Figure 4. Structure-based drug design of the class VIII inhibitors. (**A**) Schematic representation of the binding mode of hit compound **1** (aquamarine sticks) with huBChE (PDB ID 4TPK). The residues of the acyl-binding pocket are shown as gray sticks. The Tyr332 that can form the crucial cation-π interactions is shown as green sticks. Possible interactions (hydrogen bonds and/or cation-π interactions) with catalytic residues (purple sticks) and Trp82 (orange sticks) are shown as yellow dashes. (**B**) The modifications to compound **1** that were introduced during this design step are indicated in red.

In vitro Cholinesterase Inhibitory Activities and Structure–Activity Relationships

The synthesized compounds were first evaluated for their relative inhibition of recombinant huBChE hydrolase activity, using the BChE-specific substrate butyrylthiocholine iodide and the method of Ellman.[46] The inhibitory potencies against murine AChE (mAChE) were determined for all of the synthesized compounds using the specific AChE substrate acetylthiocholine iodide. mAChE was chosen as the surrogate for human AChE since the distribution of the amino-acid

residues along the active site gorge of these two enzymes is strictly conserved.[47] The IC_{50} values were determined for all of the compounds that showed at least 50% relative inhibition at 10 μM, whereas the other compounds were classified as inactive (IC_{50} >10 μM). Table 1 lists the structures, inhibitory potencies (i.e., IC_{50}) and selectivities towards huBChE [i.e., IC_{50} (mAChE)/ IC_{50} (huBChE)] of the most potent of these **class I–VIII** inhibitors. Supporting Table S1 provides the data that were obtained with all 49 of the amides produced in the present study. The inhibitory potencies and selectivities toward BChE of initial hit compound **1** and sulfonamide **2** are indicated in Table 1 for comparison.

Altogether, these data highlight the following concepts that are needed to preserve the huBChE inhibitory activity of these compounds: (*i*) no modification or replacement of the naphthalene-2-yl moiety, or replacement of the 2,3-dihydro-1*H*-inden moiety with a benzyl group; (*ii*) a basic (protonatable) piperidine nitrogen is essential; (*iii*) a 1,3-disubstituted piperidine is superior to a 1,4-disubsituted analog; and (*iv*) the -$(CH_2)_2$OMe chain can only be replaced by a -$(CH_2)_2NMe_2$ group, which greatly improves the inhibitory potency. Further details regarding the structure–activity relationship of these compounds can be found in the Supporting Discussion.

Compound **3** was the most potent inhibitor of this series, and therefore the only one that was further evaluated for biological activity. In all of these biological studies, compound **3** was used in the form of its hydrochloride salt (**3 dichloride**) (Supporting Figure S8), with the exception of the enzyme kinetics studies, in which compound **3** was used as its free base.

Table 1. Structures and inhibitory potencies of hit compound 1, sulfonamide 2, and the most potent of the type I–VIII inhibitors.

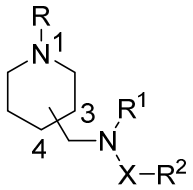

N°	Inhibitor class	Piperidine disubstitution pattern	Subsitution				IC_{50} ±SEM (μM)[a]		Selectivity ratio[b]
			R	R^1	X	R^2	huBChE	mAChE	
1	Initial hit	1,3		$(CH_2)_2OMe$	CO	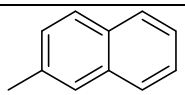	0.021 ±0.002	102.1 ±2.5	4862
2	/	1,3	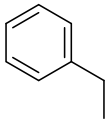	$(CH_2)_2OMe$	SO_2	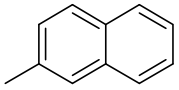	0.0049 ±0.0003	>10	>2041
3	VIII	1,3		$(CH_2)_2NMe_2$	CO	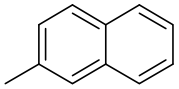	0.00103 ±0.00004[c]	>10	>9709
26	I	1,3	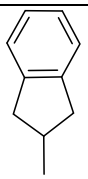	$(CH_2)_2OMe$	CO	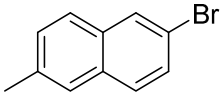	0.410 ±0.053	>10	>24
27	II	1,3	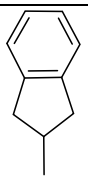	H	CO	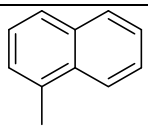	0.067 ±0.001	>10	>149
28	III	1,3	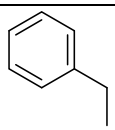	$(CH_2)_2OMe$	CO	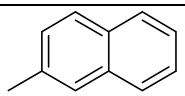	0.230 ±0.008	>10	>43

29	IV	1,3	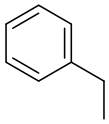	H	CO	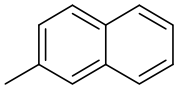	1.437 ±0.409	>10	>7
30	V	1,3	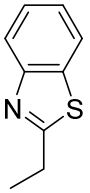	H	CO	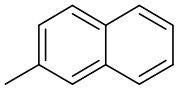	0.632 ±0.016	>10	>16
31	VI	1,3	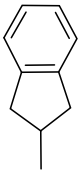	$(CH_2)_3OMe$	CO	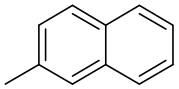	0.03824 ±0.00162	>10	>262
32	VII	1,4	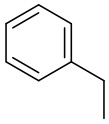	$(CH_2)_2OMe$	CO	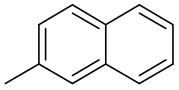	0.702 ±0.033	>10	>14
	Tacrine[35]		/	/	/	/	0.012 ±0.003	0.106 ±0.01	8.6

[a]The values are expressed as mean ± SE of at least two independent experiments.

[b]Selectivity ratio: IC_{50} (mAChE)/IC_{50} (huBChE)

[c]IC_{50} value does not reflect the true affinity due to the concentration of the huBChE surpassing the concentration of inhibitor in the *in vitro* assays. The IC_{50} value for the tight binder, compound **3**, is thus converging to the total enzyme concentration (1 nM).

Chiral HPLC Resolution and Kinetic Studies of Compound 3

Semi-preparative reversed-phase chiral HPLC (Supporting Figure S8A; Experimental Section) was used to resolve compound **3** into its pure enantiomers. The optical purities of the enantiomers were determined by calculation of the enantiomeric excess (e.e.) using analytical reversed-phased

chiral HPLC (Supporting Figure S8B, C; Experimental Section) and by the measurement of the optical rotation (Experimental Section). Both enantiomers were obtained with e.e. of 99%.

The affinity of compound **3** for its target enzyme huBChE was particularly high, such that the value of K_i was lower than the total concentration of enzyme used in the assay system (i.e., 1 nM). This situation is referred to as tight-binding inhibition, and it presents some unique challenges for the appropriate quantitative assessment of the potency of compound **3**. To determine the actual affinity of the pure enantiomers of compound **3**, the enzyme kinetic experiments were carried out on a stopped-flow apparatus according to Copeland's guidelines for evaluation of tight-binding inhibitors.[48] Briefly, the full progress curves of the formation of the enzymatic products were followed in the absence and presence of each enantiomer of compound **3**. The curves were analyzed simultaneously with the ENZO application, using a model that also accounted for the depletion of the free inhibitor concentration due to the formation of the enzyme-inhibitor complex.[49] Accordingly, a single-step competitive mechanism with a slow k_{on} (Figure 5A) allowed full reproduction of these progress curves. Of note, this mechanism is typical of most tight-binding inhibitors.[48] Curvature in the initial phase of the **(+)-3** inhibited enzyme reaction was observed, which is indicative of slow-onset of inhibition (Figure 5B).

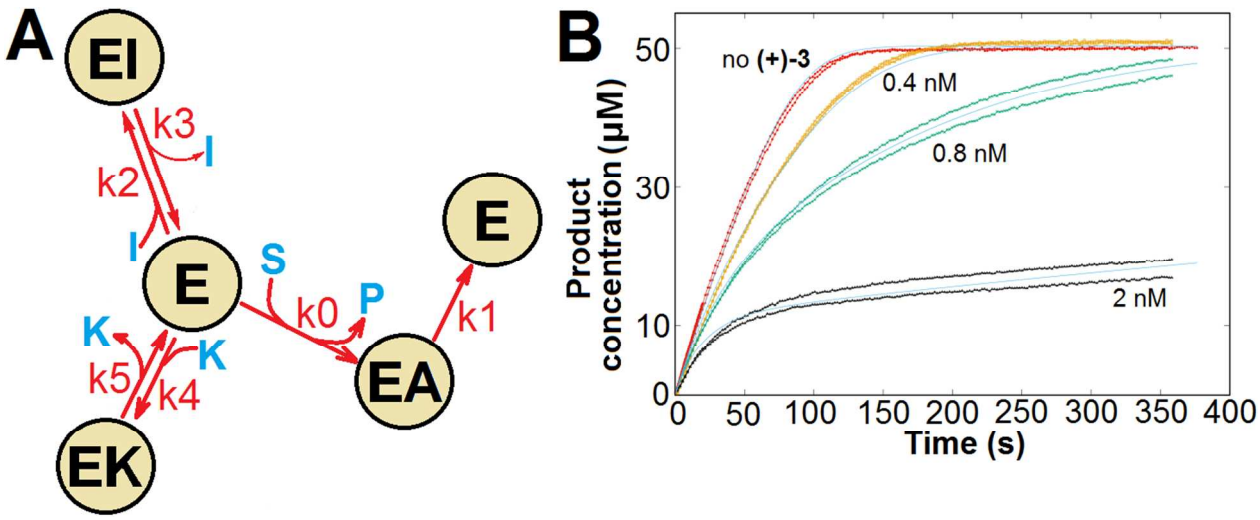

Figure 5. **Determination of the inhibition mechanism and K_i of compound (+)-3.** (**A**) Competitive single-step inhibition mechanism with slow association (low k_{on}) that fully reproduced the progress curves obtained. S, substrate; P, product; E, enzyme; EA, acylated enzyme; I, **(+)-3**; K, **(–)-3**; k0–k5, kinetic constants. (**B**) Progress curves for hydrolysis of 50.4 μM butyrylthiocholine iodide by 1.07 nM huBChE in the absence (no **(+)-3**; red curves) and presence of the pure enantiomer of compound **(+)-3** at 0.4 (orange curves), 0.8 (green curves) and 2 nM (black curves). Data were obtained using a stopped-flow apparatus. Each concentration was performed in duplicate. Fitted curves for all of the conditions are shown as smooth lines.

A more than 50-fold difference in the huBChE inhibitory potencies was seen between the pure enantiomers, with the eutomer of compound **3**, compound **(+)-3**, showing a particularly low inhibition constant (11.1 pM). The determined rates and the calculated inhibition constants for each of the enantiomers, along with the K_m and k_{cat} values for butyrylthiocholine iodide, are listed in Table 2. The k_{on} values of substrates and small inhibitors are in the range of 10^8 to 10^9 $M^{-1}s^{-1}$, respectively and do not differ substantially. On the other hand, the k_{off} value reflects all interactions between the ligand and the protein, and depends on the availability of the compound,

in this case the two enantiomers, to realize as many interactions (binding energy) as sterically possible.

Table 2. Characteristic kinetic constants for the hydrolysis of butyrylthiocholine iodide (BTCI) by huBChE, and its inhibition by compounds **1**, **3** and bis-tacrine at pH 8. The values are expressed as mean ± SE of at least two independent experiments.

Compound	**Kinetic constant**				
	K_m (μM)	**k_{cat} (s^{-1})**	**K_i (pM)**	**k_{on} ($M^{-1}s^{-1}$)**	**k_{off} (s^{-1})**
BTCI	12	859	--	--	--
(–)-**3**	--	--	603 ± 35.7	$1.02 \pm 0.02 \times 10^{8}$	$6.17 \pm 0.22 \times 10^{-2}$
(+)-**3**	--	--	10.8 ± 0.46	$1.49 \pm 0.02 \times 10^{8}$	$1.60 \pm 0.05 \times 10^{-3}$
(+)-**1**	--	--	2710 ± 31.4 [35]	2.11 ± 0.01 × 10^{7} [35]	$5.72 \pm 0.03 \times 10^{-2}$ [35]
(–)-**1**	--	--	27050 ± 1604 [35]	1.28 ± 0.04 × 10^{7} [35]	3.45 ± 0.11 × 10^{-1} [35]
Bis(7)-tacrine[50,51]	--	--	163 ± 6	$1.85 \pm 0.04 \times 10^{8}$	0.030 ± 0.0006

Crystal Structure of HuBChE in Complex with Compound 3

The co-crystal structure of compound **3** with huBChE was solved at 2.1 Å resolution. The crystals of huBChE in complex with compound **3** were obtained by co-crystallization methods. This involved setting hanging drops after pre-incubation of 500 μM compound **3** dichloride in 1% dimethylsulfoxide aqueous solution with the enzyme solution (90 μM) for 3 h. Although

racemic compound **3** was used for the experiments, the observed electronic density suggests that the *R* isomer was bound in the active site. This assumption is based on the local environment, which provides the *R* isomer with an extra hydrogen bond between the piperidine nitrogen of compound **3** and a surrounding water molecule (127). Examination of the binding mode explains the exceptional binding affinity of the inhibitor compound **3** towards huBChE (Figure 6). Similar to the parent hit of compound **1**, the naphthalene ring is T-stacked with Trp231 in the acyl-binding pocket of huBChE. The fact that this pocket is comparatively smaller in AChE[50] likely explains why compound **3** displays high selectivity towards huBChE over mAChE (Table 1). Furthermore, the piperidine nitrogen forms a cation-π interaction with the indole ring of Tyr332. The $-(CH_2)_2NMe_2$ side chain replaces the $-(CH_2)_2OMe$ chain of hit compound **1**, and points toward the choline-binding pocket. The tertiary amine forms a cation-π interaction with Trp82, with a distance of 3.7 Å to the closest carbon of the indole ring. This additional interaction of compound **3** can be clearly correlated with its picomolar inhibitory potency. This thus validates the rational drug-design approach undertaken on the basis of the previous structural data, which resulted in this increased inhibitory potency.

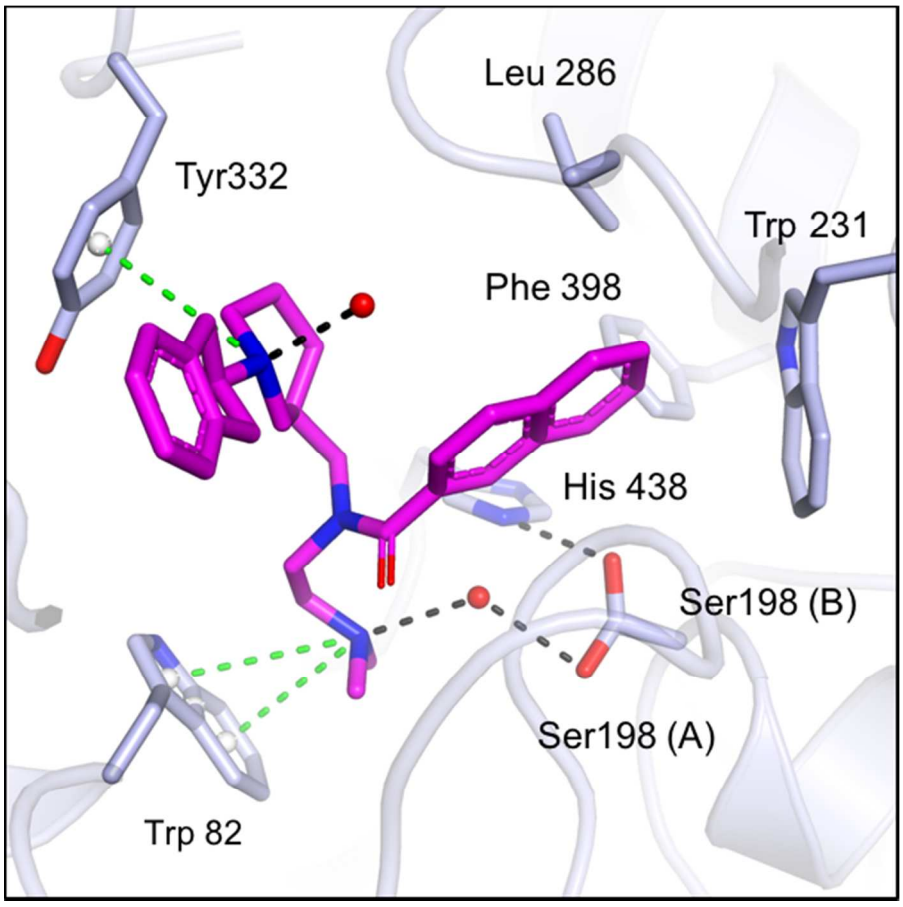

Figure 6. Crystal structure of compound 3 (*R* isomer) in complex with huBChE (PDB ID 5NN0). Compound **3** (magenta) and the key residues of huBChE involved in the binding are shown as sticks, as are the catalytic residues (i.e., His438, Ser198). Note that Ser198 was observed in the crystal in two alternate conformers. Trp231, Phe398, and Leu286 form the acyl-binding pocket, into which the naphthalene ring of compound **3** fits. Water molecules are presented as red spheres, hydrogen bonds are black, and cation-π interactions are green dashes between the positively charged nitrogen atom and the center of the aromatic rings. The piperidine nitrogen forms a cation-π interaction with Tyr 332 (4.6 Å), while the tertiary amine (-$(CH_2)_2NMe_2$) of compound **3** is 4.2 Å and 4.4 Å from the benzene and pyrrole rings of Trp82, respectively.

Thermodynamic and Computational Analysis of Binding

Thermodynamics of ligand binding for compounds **(+)-1** and **(+)-3** was investigated by enzyme kinetic experiments at three different temperatures (Supporting Figure S9), and thermodynamic parameters were calculated from Arrenhius plots (Supporting Figure S10). From this thermodynamic profiling the Gibbs free energies of binding (ΔG), which partition into enthalpic (ΔH) and enthropic (TΔS) binding contributions, were obtained. Compound **(+)-1** (ΔG = –49.88 kJ/mol) was found to be predominantly enthalpic binder with ΔH contribution of –46.36 kJ/mol and small favorable entropic portion of –3.52 kJ/mol. Also for compound (+)-**3** (ΔG= –60.65 kJ/mol), very strong enthalpic interactions of –97.23 kJ/mol were determined, however they were partially compensated by entropic penalty of +36.58 kJ/mol (Figure 7).

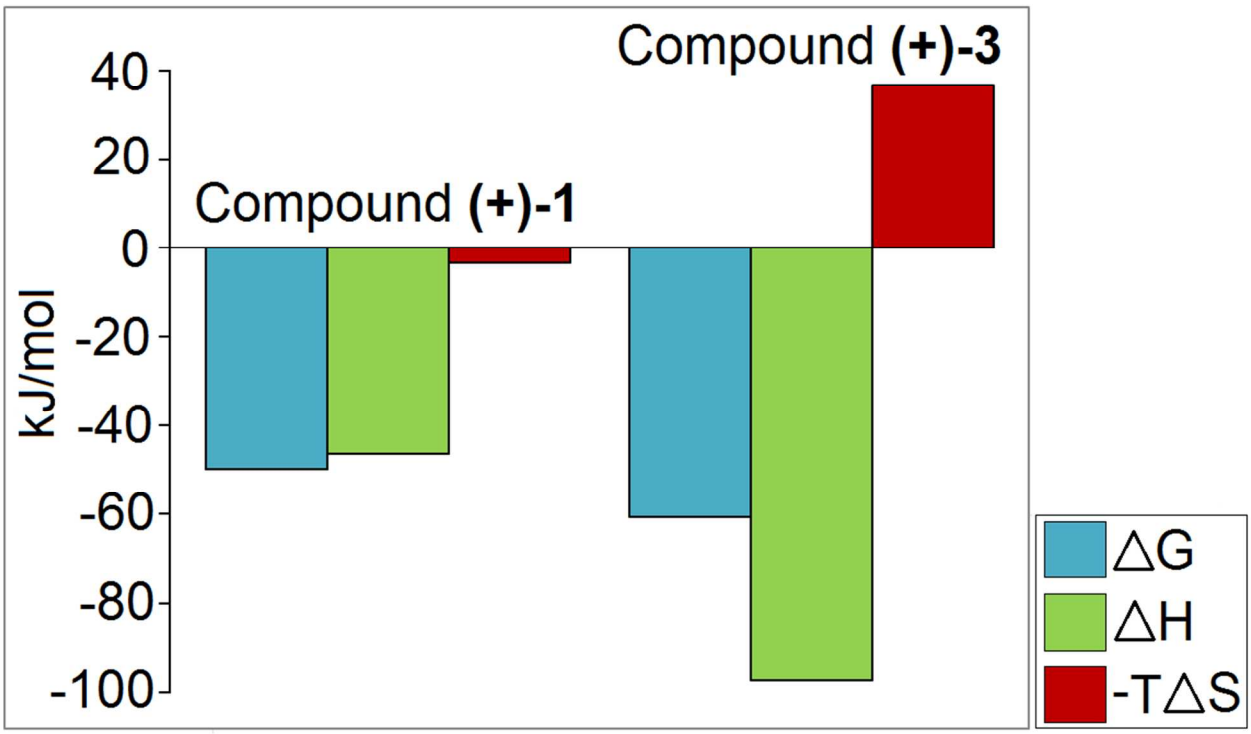

Figure 7. Thermodynamic signatures for compounds (+)-1 and (+)-3. Histograms of thermodynamic signatures of hBChE-compound complexes, with Gibbs free energy of binding (ΔG; blue), enthalpy (ΔH; green) and entropy (–TΔS; red).

These results are consistent with *in silico* analysis of binding modes and interaction energies calculations. Using Schrödinger Glide XP docking protocol, compounds **(+)-1** and **(+)-3** were scored within their respective crystal complexes, and their docking scores were –8.687 and –15.197 kcal/mol, respectively. A key difference in interaction profiles between both compounds was observed with compound **(+)-3** demonstrating favorable electrostatic/π-cation interactions (Electro and π-cat terms –1.26 and –0.91, respectively), which were not present in compound **(+)-1** (–0.72 and 0). Furthermore, while only one water-bridged H-bond was observed between methoxy group and carbonyl oxygen of compound **(+)-1** with crystal water 781 (Supporting Figure S11), a network of water molecules in a vicinity of compound (+)-**3** (crystal waters: 54, 60, 81, 97, 103, 119, 127, 148, 186, 191, 221 and 383) could be observed (Supporting Figure S12). Crystal waters 54 and 127 enable further water-bridged H-bonds (with Ser198 and His485, and Pro285, respectively), while others form a water lattice around the compound **(+)-3**. We can postulate that the observed water molecules contribute favorably to the enthalpy of binding, while simultaneously represent a high entropic penalty.

Rat Brain Slices Experiments

To confirm that compound **3** can efficiently inhibit BChE in an environment that is more similar to *in vivo* conditions, inhibition of BChE was performed in rat brain slices. The modified Koelle-Karnovsky histochemical method was used on the brain sections where the highest BChE activity was detected.[29, 52–54] The formation of the dark brown/ black granular BChE reaction product was observed in both vascular and neuronal structures of the laterodorsal thalamic nucleus. Complete BChE inhibition was observed when these sections were incubated with 10 μM compound **3** (Figure 8). Of note, 300 μM of sulfonamide **2** was needed to achieve the same effect, highlighting a correlation between the inhibition constants determined *in vitro* and the results obtained here.[29]

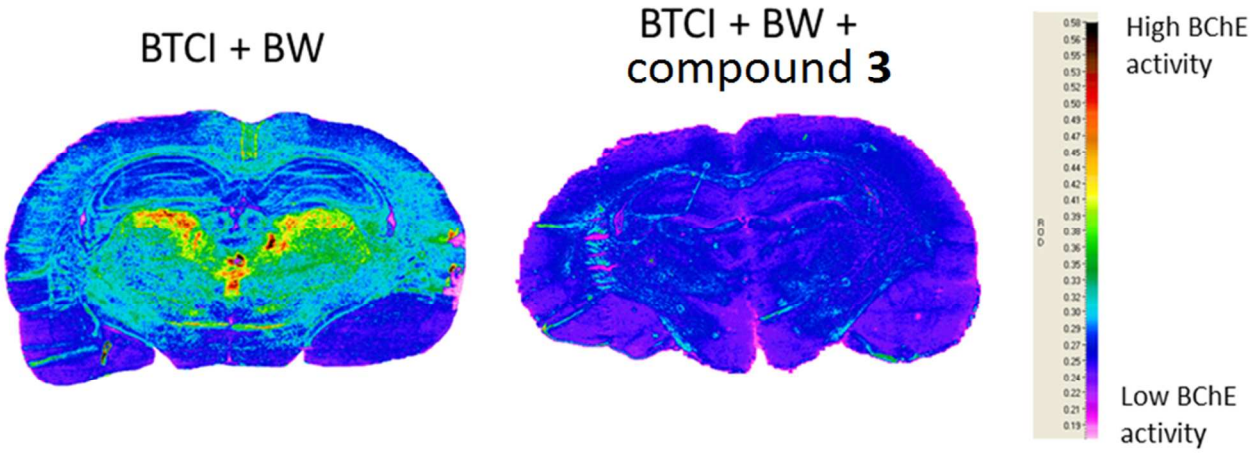

Figure 8. Representative coronal section from a rat brain in the region containing the laterodorsal thalamic nucleus. The sections were processed for BChE histochemical staining using 4 mM butyrylthiocholine iodide (BTCI), in the absence (left) and presence (right) of 10 μM compound **3**. Selective AChE inhibitor 1,5-bis(4-allyldimethylammoniumphenyl)pentan-3-one dibromide was added to completely block AChE activity. Magnification, 10×. The relative optical density scores for the staining intensity for BChE activity are shown on the right.

Cytotoxicity of Compound 3

The cytotoxicity profile in human neuroblastoma SH-SY5Y cells (Figure 9) demonstrated a LC_{50} of 6.63 μM for compound **3**, which is more than 6,000-fold greater than the concentration needed for 50% inhibition of huBChE. Cytotoxicity profile was also demonstrated in the HepG2 cell line, where compound **3** showed even lower impairment of the cell metabolic activity (LC_{50} = 33.87 μM) (Figure 9).

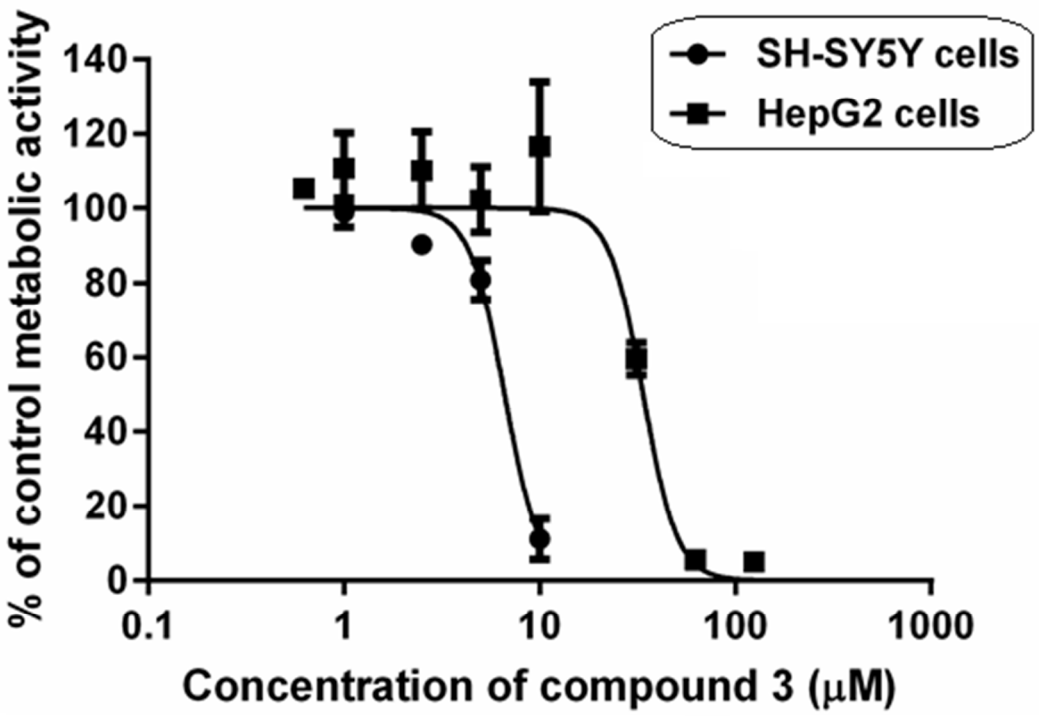

Figure 9. Cytotoxicity of compound 3. Concentration-dependent cytotoxicity of compound **3** in human neuroblastoma SH-SY5Y cells and in human hepatocellular HepG2 cells. SH-SY5Y cells and HepG2 cells were incubated in the presence of the indicated concentrations of compound **3**. Cell viability was evaluated after 48 h (for SH-SY5Y cells) and 24 h (for HepG2 cells) using the MTS assay. The control group (with DMSO) was considered as 100% cell viability. Data are means ±SD of three independent experiments, each carried out in triplicate. The X axis is in log scale.

In Vitro Pharmacokinetics and *In Vivo* Blood Plasma–Brain Distribution of Compound 3

The *in vitro* pharmacokinetics and *in vivo* blood plasma–brain distribution of compound **3** were determined as previously reported for sulfonamide **2**.[29] The permeability values (P_{app}) of compound **3** in heterogeneous human epithelial colorectal adenocarcinoma (Caco-2) cells were determined in both the absorptive [apical-to-basolateral; (A–B)] and eliminatory [basolateral-to-apical; (B–A)] directions, allowing the calculation of the efflux ratio as $P_{app(B–A)}/P_{app(A–B)}$. The $P_{app(A–B)}$ (absorptive) of compound **3** was 28.0 ±0.9 $\times 10^{-6}$ cm/s, which is classified as "high"

according to the biopharmaceutical classification system of drug permeability.[55] This would thus not be a limiting factor in the bioavailability of compound **3**. $P_{app(B–A)}$ (eliminatory) of compound **3** was 46.1 ±5.2 $\times 10^{-6}$ cm/s. These data yielded an "efflux ratio" ($P_{app(B–A)}/P_{app(A–B)}$) of 1.65, which is classified as "low" and indicates very limited active transport of compound **3** in the eliminatory direction.[56]

Further analysis showed that 93% of compound **3** was bound to plasma proteins (Supporting Table S2), which classifies this compound as highly protein bound.[57] Compound **3** was relatively stable in human plasma, with 76% still present and intact after 120 min (i.e., $t_{1/2}$ >120 min) (Supporting Table S3). Likewise, the hepatic metabolism of compound **3** in cryopreserved hepatocytes was moderate ($t_{1/2}$ >120 min) (Supporting Table S4). Compound **3** showed a considerably longer half-life compared to other high extraction ratio reference compounds cleared by the cytochrome P450 enzymes used as positive controls in the metabolic stability assays (i.e., flurazepam, naloxone, propranolol; Supporting Table S5). The moderate hepatocyte clearance (<8.2 μL/min/million cells) (Supporting Table S4) of compound **3** is in agreement with the long half-life and single metabolite (monomethyl derivative **11**; Supporting Table S6) identified using liquid chromatography–high resolution mass spectrometry. As metabolite **11** is a potent and selective huBChE inhibitor (IC_{50} = 0.018 μM), the parent compound **3** might have residual pharmacological activity.

As AD is a brain disorder, any drug used for its treatment needs to cross the blood–brain barrier. *In vivo* measurements of the distribution between the blood plasma and the central nervous system is the most reliable evaluation of this crossing of the blood–brain barrier.[58] One hour after rats had an intraperitoneal injection of 10 mg/kg compound **3**, the mean (±SEM) concentration of compound 3 in the brain tissue was 248 ±37 μg/kg, while that in the blood

plasma was 169 ±13 μg/L. The brain-to-blood plasma ratio of compound **3** was 1.47, which is more than three-fold higher than the brain-to-blood plasma ratio of sulfonamide **2**.[29]

In Vivo Activity of Compound 3

Encouraged by the selective and potent huBChE inhibitory activity, inhibition of BChE in rat brain slices, low cytotoxicity, favorable *in vitro* pharmacokinetics, and proven penetration into the brain, we set out to test the effects of compound **3** on behavioral activities. The Morris water maze task was performed to test the potential procognitve properties of compound **3**.

Scopolamine was used to induce cognitive deficits in test animals (1 mg/kg; intaperitoneal injection prior to the acquisition trials in each test). Scopolamine is a non-selective muscarinic ACh receptor antagonist, and it produces cognitive deficits in test subjects that are comparable to those caused by the cholinergic deficit characteristic of AD.[59–62] ChE inhibitors alleviate scopolamine-induced cognitive deficits by increasing the levels of synaptic ACh (notably in the brain), which results in displacement of scopolamine from muscarinic ACh receptors.[60,63] Scopolamine-induced amnesia is thus frequently used in AD research for preclinical evaluation of pro-cognitive properties of ChE inhibitors.[59,64–67] The selective AChE inhibitor donepezil was used in the behavioral tasks as the positive control. C57BL/6J and CD-1 Krf mice were used for the experiments. These mice have an unaltered brain BChE/AChE enzymatic activity ratio, and they were used because test animals with an increased BChE/AChE enzymatic activity ratio are currently not available.

The Morris water maze task is a hippocampus-dependent memory and spatial learning task used to investigate (*i*) effects on long-term memory, through decreased time to reach an escape platform (i.e., escape time latency); (*ii*) effects on cognition through the measure of the overall distance travelled to reach the escape platform; and (*iii*) induction of sensorimotor deficits

through the measure of the mean speed of swimming.[68–70] During the consecutive training days in all of experimental groups, the escape latency times progressively decreased, as evident from the characteristic learning curves (Figure 10A). Scopolamine-treated mice showed significantly attenuated learning abilities and cognitive functions, as compared to vehicle-treated mice, as they had significantly longer escape latency times (Figure 10A) and travelled longer distances to reach the escape platform (Figure 10B). This cognitive dysfunction caused by scopolamine was attenuated by compound **3** (30 mg/kg, intraperitoneally) as demonstrated by both shorter escape latency times (Figure 10A) and shorter distances travelled to reach the escape platform (Figure 10B). This thus illustrates the memory-improving and procognitive properties of compound **3**, which were comparable to sulfonamide **2**.[29] Donepezil (10 mg/kg) was also effective in this behavioral test (Figure 10A, B). This was expected, as donepezil is a selective AChE inhibitor and compound **3** is a selective BChE inhibitor, and the mice used had an unaltered brain BChE/AChE enzymatic activity ratio, with AChE accounting for the majority of their brain ChE enzymatic activity.

Analysis of the mean speed of swimming revealed that scopolamine induced significant hyperlocomotion in mice, as it increased the mean speed of swimming (vehicle, 0.13 m/s; scopolamine 0.20 m/s). Both compound **3** and donepezil decreased the hyperlocomotion caused by scopolamine, as they reduced the mean speed of swimming compared to scopolamine-treated mice (scopolamine + compound **3**, 0.18 m/s; scopolamine + donepezil, 0.15 m/s).

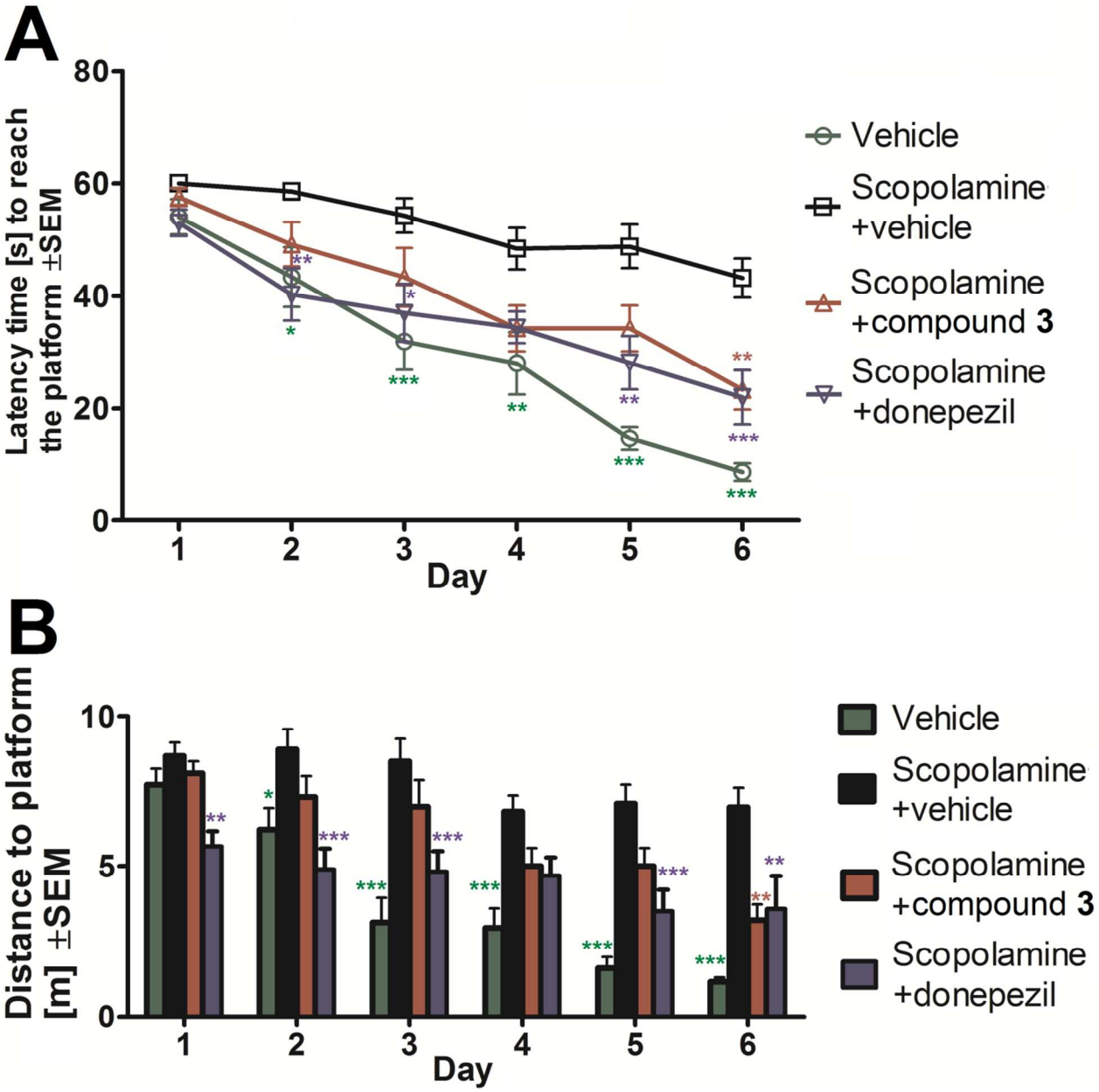

Figure 10. Effects of compound 3 and donepezil on scopolamine-induced memory impairment in the Morris water maze task. (**A**) Learning curves of the escape latencies for vehicle-treated mice (green), scopolamine-treated control mice (black), and scopolamine-induced memory-impaired mice treated with 30 mg/kg compound **3** (brown) or 10 mg/kg donepezil (purple) during the acquisition phase. (**B**) Distances traveled to reach the target platform during the acquisition phase in vehicle-treated mice (green bars), scopolamine-treated control mice (black bars), and scopolamine-induced memory-impaired mice treated with 30 mg/kg compound **3** (brown bars) or 10 mg/kg donepezil (purple bars). Data are means ±SEM.

Statistical analysis: repeated-measures ANOVA, followed by Bonferroni *post-hoc* comparisons. * $p < 0.05$; ** $p < 0.01$; *** $p < 0.001$ (vs. scopolamine + vehicle-treated mice).

In Vivo Safety of Compound 3

Peripheral adverse effects of approved drugs for the treatment of patients with AD are the result of an excess of ACh produced by inhibition of ChEs in the peripheral nervous system, the parasympathetic autonomic system, and the basal ganglia.[31] To interpret the data from the Morris water maze task, the *in vivo* safety profile of compound **3** and its impact on the general activity and motor skills of the mice were determined, using the locomotor activity and rotarod tests. Compound **3** was tested at the concentration effective in the behavioral tests (30 mg/kg intraperitoneal). Compound **3** did not induce motor deficits in these mice, as shown in the rotarod tests, at 6 rpm, 18 rpm, or 24 rpm. Although compound **3** reduced the locomotor activity between 24 min and 30 min (Supporting Figure S13) of the locomotor activity test, this had no impact on the results obtained in the behavioral test. Additionally, administration of compound **3** to mice did not produce any acute adverse cholinergic effects. This was expected, as selective BChE inhibition *in vivo* does not produce peripheral (parasympathomimetic) adverse effects.[29,31]

Conclusions

A comprehensive series of 49 selective BChE inhibitors was designed and synthesized, and their structure–activity relationships were determined. Crystal-structure-based design led to the most potent inhibitor of the series, compound **3**, which was resolved into its pure enantiomers using semi-preparative chiral HPLC. Detailed kinetic studies showed slow, tight-binding inhibition of compound **3** *versus* huBChE, where the eutomer demonstrated a picomolar *in vitro* huBChE inhibitory potency (K_i = 11.1 pM). The solved crystal structure of compound **3** in complex with

huBChE revealed two cation-π interactions that were crucial for this good inhibitory potency. Additionally, compound **3** inhibited BChE in rat brain and was not cytotoxic. *In vitro* pharmacokinetic experiments showed compound **3** was highly protein bound, and stable in human plasma and hepatocytes, and showed its "high" permeability in Caco-2 cells. Finally, compound **3** crossed the blood–brain barrier *in vivo*, and improved memory, cognitive functions and learning abilities of mice with scopolamine-induced amnesia. Considering these properties, compound **3** represents a promising advanced lead compound for the developing drugs for treatment of patients with AD.

Experimental Section

General Chemistry Methods

Chemicals and solvents were obtained from commercial sources (i.e., Acros Organics, Alfa Aesar, Fluka, Merck, Sigma-Aldrich, TCI Europe), and were used without purification, unless otherwise stated. Reactions were monitored using analytical thin-layer chromatography plates (Merck 60 F254, 0.20 mm) and the components were visualized with ultra-violet light and/or through staining with ninhydrin reagent solution. Evaporation of solvents was performed at reduced pressure. Flash column chromatography was performed on silica gel 60 (0.040-0.063 mm) for column chromatography (particle size, 230-400 mesh). ^{1}H-NMR and ^{13}C-NMR were recorded on a Bruker Avance III NMR 400 MHz spectrophotometer at 400.130 and 100.613 MHz, respectively, and 295 K, unless otherwise stated. The chemical shifts (δ) are reported in parts per million (ppm) and are referenced to the deuterated solvent used. The coupling constants (*J*) are reported in Hz, and the splitting patterns are indicated as: s (singlet), bs (broad singlet), d (doublet), bd (broad doublete), dd (doublet of doublets), td (triplet of doublete), t (triplet), bt (broad triplet), dt (doublet of triplets), q (quartet) and m (multiplet). Optical rotations were

measured on a Perkin-Elmer 241 MC polarimeter. The reported values for specific rotation are the mean values of 10 successive measurements using an integration time of 5 s. Infrared spectra were obtained on a Perkin-Elmer FT-IR System Spectrum BX or on a Thermo Nicolet. Mass spectra were recorded on a VG-Analytical AutoSpec Q Micromass mass spectrometer at Jožef Stefan Institute, Ljubljana, Slovenia. Analytical reversed-phase HPLC (methods A and B), semi-preparative reversed-phase chiral HPLC (method C) and analytical reversed-phase chiral HPLC (method D) were performed on an LC modular system (Agilent 1100) equipped with an autosampler, a quarternary pump system, a photodiode array detector, a thermostated column compartment, a fraction collector compartment, and the ChemStation data system. Analytical reversed-phase HPLC method E was performed on an LC system (Dionex Ultimate 3000 Binary Rapid Separation; Thermo Scientific) equipped with an autosampler, a binary pump system, a photodiode array detector, a thermostated column compartment, and the Chromeleon Chromatography Data System. The detector on both HPLC systems was set to 210 nm, 254 nm, and 280 nm. The column used for methods A and B was a C18 analytical column (150 × 4.6 mm, 5 μm; Zorbax Eclipse Plus; Agilent). The column used for method E was a C18 analytical column (250 × 4.6 mm, 5 μm; Phenomenex Gemini C18). For both of these columns, an HPLC guard cartridge system was used (octadecyl; 4.0 × 3.0 mm ID; Security Guard Cartridge C18 CODS; Phenomenex). The column used for reversed-phase chiral HPLC methods C and D was a Kromasil 5-CelluCoat RP column (250 × 10 mm). A guard cartridge was used with this column, as a Kromasil 5-CelluCoat RP (10-21.2 mm). All of the HPLC columns were thermostated at 25 °C.

Method A: The sample solution (10 μL; 0.1 mg/mL in MeCN) was injected and eluted at a flow rate of 1 mL/min, using a linear gradient of mobile phase A (70% [v/v] 10 mM aqueous phosphate buffer, pH 8.00, in MeCN) and mobile phase B (30% [v/v] 10 mM aqueous phosphate

buffer, pH 8.00, in MeCN). The gradient for method A (for mobile phase B) was: 0–7 min, 0%–100%; 7–17 min, 100%, 17–20 min, 100%–0%.

Method B: The sample solution (10 μL; 0.1 mg/mL in MeCN, except for **3 dichloride** which was dissolved in H_2O) was injected and eluted at a flow rate of 1 mL/min, using a linear gradient of mobile phase A (0.1% [v/v] TFA 10 mM aqueous solution) and mobile phase B (MeCN). The gradient for method A (for mobile phase B) was: 0–15 min, 10%–90%; 15–20 min, 90%, 20–21 min, 90%–10%.

Method C: The sample solution of compound **3** (50 μL; 25 mg/mL in acetonitrile [MeCN]) was injected and eluted over 60 min at a flow rate of 5 mL/min, using aqueous sodium borate buffer (20 mM, pH 9.00) containing 40% MeCN.

Method D: The sample solution of enantiomer of compound **3** (100 μL; 1 mg/mL in acetonitrile [MeCN]) was injected and eluted over 43 min at a flow rate of 5 mL/min, using aqueous sodium borate buffer (20 mM, pH 9.00) containing 40% MeCN.

Method E: The sample solution (10 μL; 0.2 mg/mL in MeOH) was injected and eluted at a flow rate of 1.5 mL/min, using a gradient of mobile phase A (0.1% TFA) and mobile phase B (MeOH). The gradient for method E (for mobile phase B) was: 0–20 min, 40%; 20–21 min, 40%-90%: 21–25 min, 90%.

General Synthetic Procedures

The general procedure for formation of amide bond using acyl chlorides (general procedure 1)

The amine (1.0 equiv.), 2,2,2-trifluoroacetate salt of amine (1.0 equiv.), or chloride salt of amine (1.0 equiv) was dissolved or suspended in CH_2Cl_2 and cooled to 0 °C. The reaction mixture was stirred and trimethylamine (Et_3N) (1.0 equiv. for amine and (1.0 + n) equiv. for 2,2,2-trifluoroacetate or chloride salt of amine [n being the molar quantity of 2,2,2-trifluoroacetate or

chloride in the salt]) was added drop-wise. After 15 min, acyl chloride (1.0 equiv.) was added, and the mixture was allowed to warm to room temperature and then stirred for 24 h. The reaction mixture was transferred into a separating funnel, washed with water followed by 0.5 M aqueous HCl solution for non-amine products, then saturated aqueous $NaHCO_3$ solution, dried over anhydrous Na_2SO_4, and evaporated. The crude product was purified by flash column chromatography.

General procedure for formation of amide bond using coupling reagent TBTU (general procedure 2)

The carboxylic acid (1.0 equiv) was dissolved or suspended in CH_2Cl_2 at room temperature. The reaction mixture was stirred and trimethylamine (Et_3N) (2.0 equiv. for amine and (2.0 + n) equiv. for 2,2,2-trifluoroacetate or chloride salt of amine [n being the molar quantity of 2,2,2-trifluoroacetate or chloride in the salt]) was added drop-wise. After 5 min, TBTU (1.0 equiv.) was added and the reaction mixture was stirred for 30 min before the amine (1.0 equiv.; 2.0 equiv. when N^1,N^1-dimethylethane-1,2-diamine and N^1,N^1-dimethylpropane-1,3-diamine were used), 2,2,2-trifluoroacetate salt of amine (1.0 equiv.) or chloride salt of amine (1.0 equiv) was added. After 24 h, the reaction mixture was transferred into a separating funnel, washed with water followed by 0.5 M aqueous HCl solution for non-amine products, then saturated aqueous $NaHCO_3$ solution, dried over anhydrous Na_2SO_4, and evaporated to produce the crude amines, which were either used in the next step without further purification or were purified by flash column chromatography or precipitation.

General procedure for amide bond reduction with $LiAlH_4$ (general procedure 3)

To a three-neck round-bottomed flask equipped with a stirring bar and a reflux condenser, $LiAlH_4$ (5.0 equiv. calculated to the crude amide) and anhydrous THF were added under an argon atmosphere. A solution of crude amide (1.0 equiv.) in anhydrous THF was added with a double-tipped needle, and the reaction mixture was refluxed for 3 h. The mixture was then cooled to 0 °C, quenched by drop-wise addition of H_2O (*n* g $LiAlH_4$ required *n* mL H_2O), 15% aq. NaOH (*n* g $LiAlH_4$ required *n* mL 15% aq. NaOH) and H_2O (*n* g $LiAlH_4$ required 3*n* mL H_2O). After vigorous stirring for 1 h at room temperature, the suspension was filtered and the precipitate washed thoroughly with THF. The combined filtrates were evaporated to produce the crude amine, which was used in the next step without further purification.

General procedure for introduction of Boc-protective group (general procedure 4)

The crude amine (1.0 equiv) was dissolved in CH_2Cl_2 and cooled to 0 °C. The solution was stirred and trimethylamine (Et_3N) (1.0 equiv) was added drop-wise, followed by drop-wise addition of Boc_2O (1.0 equiv) solution in CH_2Cl_2. The reaction mixture was allowed to warm to room temperature and stirred for 24 h. The mixture was then transferred into a separating funnel, washed with water followed by saturated aqueous $NaHCO_3$ solution, dried over anhydrous Na_2SO_4, and evaporated to produce the crude carbamate, which was purified by flash column chromatography.

General procedure for removal of benzyl protective group (general procedure 5)

The benzyl amine (1.0 equiv.) was dissolved in MeOH at room temperature. The solution was stirred and agitated with a stream of argon for 30 min. $Pd(OH)_2$ on carbon (20 wt.%) (20% mass of benzyl amine) was added, followed by cyclohexene (10.0 equiv.). The resulting suspension was refluxed under an atmosphere of argon for 24 h, then filtered under suction through a pad of

Celite, and evaporated to produce the crude amine, which was used in the next step without further purification.

General procedure for reductive amination with 1H-inden-2(3H)-one (general procedure 6)

The secondary amine (1.0 equiv.) was dissolved in DCE at room temperature. The solution was stirred and agitated with a stream of argon for 15 min. $NaBH(OAc)_3$ (1.875 equiv.), 1*H*-inden-2(3*H*)-one (1.0 equiv.), and AcOH (1.0 equiv.) were added, and the resulting suspension was stirred under an atmosphere of argon for 24 h. The reaction mixture was opened to the air and quenched with saturated aqueous $NaHCO_3$ solution. The mixture was transferred into a separating funnel, and DCM was added. The separating funnel was shaken vigorously, and the organic phase was separated, dried over anhydrous Na_2SO_4, and evaporated to produce the crude amine, which was purified by flash column chromatography.

General procedure for removal of Boc-protective group (general procedure 7)

The carbamate (1.0 equiv.) was dissolved in CH_2Cl_2 at room temperature. The solution was stirred and TFA (20.0 equiv.) was added drop-wise. After 24 h, the reaction mixture was evaporated. After evaporation of the solvent, Et_2O was added to the oily residue, and the flask was placed in an ultrasonic bath until the oily residue transformed into a white solid. The flask was removed from the ultrasonic bath and the precipitate was allowed to settle to the bottom of the flask. The supernatant was removed, Et_2O was added, and the flask was placed back in the ultrasonic bath for 1 min. This procedure was repeated three times and the solid residue was dried at reduced pressure, to produce the crude product, which was used in the next step without further purification.

Declaration of Purity

All assayed final compounds were ≥95% pure as determined by HPLC.

Synthesis and Experimental Properties of Class VIII Inhibitors and Intermediates in Their Synthesis

(±)-N-((1-(2,3-Dihydro-1H-inden-2-yl)piperidin-3-yl)methyl)-N-(2-(dimethylamino)ethyl)-2-naphthamide (3)

Synthesized from crude (±)-N^1-((1-(2,3-dihydro-1*H*-inden-2-yl)piperidin-3-yl)methyl)-N^2,N^2-dimethylethane-1,2-diamine tris(2,2,2-trifluoroacetate) (**18**) (2.668 g, 4.177 mmol) and 2-naphthoyl chloride via general procedure 1. Purified by flash column chromatography using CH_2Cl_2/MeOH/Et_3N (120:10:1, v/v) as the eluent to produce 1.268 g **3** as a golden oil (67% yield). R_f = 0.28 (CH_2Cl_2/MeOH/Et_3N, 100:10:1, v/v). IR (ATR): 2931, 2767, 1625, 1476, 1422, 1285, 1135, 862, 821, 742 cm^{-1}. ^1H NMR (400 MHz, DMSO-d6, 80 °C): δ = 0.95 (bs, 1 H), 1.43–1.51 (m, 1 H), 1.59–1.67 (m, 2 H), 1.81 (bs, 1 H), 1.98–2.09 (m, 7 H), 2.70–2.83 (m, 4 H), 2.96–3.21 (m, 6 H), 3.35–3.45 (m, 4 H), 7.09–7.20 (m, 4 H), 7.41–7.43 (m, 1 H), 7.55–7.59 (m, 2 H), 7.87 (s, 1 H), 7.94–7.98 (m, 3 H). ^{13}C NMR (100 MHz, $CDCl_3$): δ = 24.83, 24.91, 28.50, 28.63, 29.64, 35.38, 36.90, 43.03, 45.55, 45.66, 47.28, 48.18, 51.94, 53.54, 55.65, 56.19, 56.72, 57.69, 66.94, 67.13, 124.03, 124.30, 124.33, 125.95, 126.36, 126.61, 126.82, 127.77, 128.24, 128.28, 132.63, 133.33, 134.19, 141.44, 172.16, 172.38. HRMS (ESI+): *m/z* calcd for $C_{30}H_{38}N_3O$ 456.3015; found 456.3008. HPLC purity, 99% at 254 nm (method B, t_R = 9.29 min).

(±)-N-((1-(2,3-Dihydro-1H-inden-2-yl)piperidin-3-yl)methyl)-N-(2-(dimethylamino)ethyl)-2-naphthamide dichloride (3 dichloride)

To a 100-mL round-bottomed flask equipped with a stirring bar, **3** (1.172 g, 2.572 mmol, 1.0 equiv.) and MeOH (60 mL) were added at room temperature. The solution suspension was stirred and agitated with a stream of argon for 15 min, and then cooled to 0 °C. Then a 2 M solution of HCl in Et_2O (5.150 mL, 10.288 mmol, 4.0 equiv.) was added drop-wise with a glass syringe. After 15 min, the reaction mixture was allowed to warm to room temperature and stirred for an additional 90 min. After evaporation of the solvent, Et_2O (50 mL) was added to the oily residue, and the flask was placed in an ultrasonic bath until the oily residue transformed into a white solid. The flask was removed from the ultrasonic bath and the precipitate was allowed to settle to the bottom of the flask. The supernatant was removed, Et_2O (60 mL) was added, and the flask was placed back in the ultrasonic bath for 1 min. This procedure was repeated three times and the solid residue was dried at reduced pressure, to produce 1.335 g **3 dichloride** as a white solid (98% yield). HPLC purity, 99% at 254 nm (method B, t_R = 9.31 min).

(±)-1-Benzoyl-N-(2-(dimethylamino)ethyl)piperidine-3-carboxamide (6)

Synthesized from (±)-1-benzoylpiperidine-3-carboxylic acid[45] (**5**) (17.000 g, 72.876 mmol) and N^1,N^1-dimethylethane-1,2-diamine via general procedure 2, to produce 20.190 g crude **6** as a yellow oil (93% yield). This product was used in the next step without further purification. R_f = 0.19 (CH_2Cl_2/MeOH, 9:1, v/v). HRMS (ESI+): *m/z* calcd for $C_{17}H_{26}N_3O_2$ 304.2025; found 304.2018.

(±)-1-Benzoyl-N-(3-(dimethylamino)propyl)piperidine-3-carboxamide (7)

Synthesized from (±)-1-benzoylpiperidine-3-carboxylic acid[45] (**5**) (6.449 g, 27.650 mmol) and N^1,N^1-dimethylpropane-1,3-diamine via general procedure 2, to produce 7.955 g crude **7** as a

golden-yellow oil (93% yield). This product was used in the next step without further purification. HRMS (ESI+): *m/z* calcd for $C_{18}H_{28}N_3O_2$ 318.2182; found 318.2181.

(±)-N^1-((1-Benzylpiperidin-3-yl)methyl)-N^2,N^2-dimethylethane-1,2-diamine (8)

Synthesized from crude (±)-1-benzoyl-*N*-(2-(dimethylamino)ethyl)piperidine-3-carboxamide (**6**) (7.000 g, 23.071 mmol) via general procedure 3, to produce 4.239 g crude **8** as colorless oil (67% yield). This product was used in the next step without further purification. R_f = 0.04 (CH_2Cl_2/MeOH, 9:1, v/v + 0.3% Et_3N). HRMS (ESI+): *m/z* calcd for $C_{17}H_{30}N_3$ 276.2440; found 276.2439.

(±)-N^1-((1-Benzylpiperidin-3-yl)methyl)-N^3,N^3-dimethylpropane-1,3-diamine (9)

Synthesized from crude (±)-1-benzoyl-*N*-(3-(dimethylamino)propyl)piperidine-3-carboxamide (**74**) (7.955 g, 25.061 mmol) via general procedure 3, to produce 5.622 g crude **76** as a slightly golden liquid (78% yield). This product was used in the next step without further purification. HRMS (ESI+): *m/z* calcd for $C_{18}H_{32}N_3$ 290.2596; found 290.2594.

(±)-N-((1-Benzylpiperidin-3-yl)methyl)-N-(2-(dimethylamino)ethyl)-2-naphthamide (10)

Synthesized from crude (±)-N^1-((1-benzylpiperidin-3-yl)methyl)-N^2,N^2-dimethylethane-1,2-diamine (**8**) (0.152 g, 0.552 mmol) and 2-naphthoyl chloride via general procedure 1. Purified by flash column chromatography using CH_2Cl_2/MeOH/Et_3N (120:8:1, v/v) as the eluent to produce 0.092 g **10** as a colorless oil (39% yield). R_f = 0.19 (CH_2Cl_2/MeOH/Et_3N, 120:8:1, v/v). IR (ATR): 2933, 2767, 1624, 1453, 1422, 1283, 1135, 1027, 821, 744, 699 cm^{-1}. ^1H NMR (400 MHz, $CDCl_3$): δ = 0.90 (d, J = 202.7 Hz, 1 H), 1.74–1.98 (m, 9 H), 2.06–2.17 (m, 1 H), 2.28–2.38 (m, 3 H), 2.61–2.90 (m, 3 H), 3.28 (bs, 2 H), 3.40–3.70 (m, 4 H), 7.21 (bs, 1 H), 7.29–7.42

(m, 5 H), 7.53 (bs, 2 H), 7.70–7.91 (m, 4 H). ^{13}C NMR (100 MHz, $CDCl_3$): δ = 24.54, 24.79, 28.16, 28.48, 34.90, 35.23, 42.99, 45.45, 45.61, 47.25, 48.01, 53.31, 53.51, 53.77, 54.40, 56.58, 57.30, 57.58, 63.33, 63.43, 123.99, 124.36, 124.39, 125.77, 126.34, 126.50, 126.73, 126.95, 127.72, 128.16, 129.05, 129.29, 132.57, 133.26, 134.15, 137.79, 138.18, 172.03, 172.26. HRMS (ESI+): *m/z* calcd for $C_{28}H_{36}N_3O$ 430.2858; found 430.2848. HPLC purity, 98% at 254 nm (method B, t_R = 8.64 min).

(±)-N-((1-Benzylpiperidin-3-yl)methyl)-N-(3-(dimethylamino)propyl)-2-naphthamide (11)

Synthesized from crude (±)-N^1-((1-benzylpiperidin-3-yl)methyl)-N^3,N^3-dimethylpropane-1,3-diamine (**9**) (0.104 g, 0.359 mmol) and 2-naphthoyl chloride via general procedure 1. Purified by flash column chromatography using CH_2Cl_2/MeOH/Et_3N (100:10:1, v/v) as the eluent to produce 0.108 g **11** as a slightly golden oil (68% yield). R_f = 0.23 (CH_2Cl_2/MeOH, 1:1, v/v). IR (ATR): 3395, 2933, 2765, 1620, 1478, 1426, 1233, 1070, 822, 746, 699 cm^{-1}. ^{1}H NMR (400 MHz, $CDCl_3$): δ = 0.91 (bd, *J* = 210.9 Hz, 1 H), 1.48–1.63 (m, 2 H), 1.77 (bs, 2 H), 1.98 (bs, 4 H), 2.23 (bs, 4 H), 2.43 (bs, 3 H), 2.62 (bd, *J* = 22.1 Hz, 1 H), 2.91 (bs, 1 H), 3.22–3.28 (m, 2 H), 3.41 (bs, 2 H), 3.47–3.66 (m, 3 H), 7.21 (bs, 1 H), 7.27–7.40 (m, 5 H), 7.54 (bs, 2 H), 7.69–7.94 (m, 4 H). ^{13}C NMR (100 MHz, $CDCl_3$): δ = 24.41, 24.48, 24.87, 26.38, 28.04, 28.06, 28.30, 34.51, 34.53, 35.00, 35.01, 42.93, 44.89, 47.31, 47.45, 52.87, 53.45, 54.23, 56.28, 56.71, 57.14, 63.24, 123.82, 124.24, 125.67, 126.31, 126.54, 126.74, 126.78, 127.05, 127.13, 127.70, 128.23, 129.12, 129.44, 132.57, 133.25, 133.99, 132.15, 137.45, 172.10. HRMS (ESI+): *m/z* calcd for $C_{29}H_{38}N_3O$ 444.3015; found 444.3010. HPLC purity, 97% at 254 nm (method B, t_R = 8.64 min).

(±)-Tert-butyl ((1-benzylpiperidin-3-yl)methyl)(2-(dimethylamino)ethyl)carbamate (12)

Synthesized from crude (±)-N^1-((1-benzylpiperidin-3-yl)methyl)-N^2,N^2-dimethylethane-1,2-diamine (**8**) (4.239 g, 15.390 mmol) via general procedure 4. Purified by flash column chromatography using CH_2Cl_2/MeOH (9:1, v/v) as the eluent to produce 3.190 g **12** as a yellow transparent oil (55% yield). R_f = 0.42 (CH_2Cl_2/MeOH, 9:1, v/v). IR (ATR): 2972, 2933, 2766, 1690, 1455, 1416, 1365, 1247, 1156, 1096, 1068, 1025, 886, 863, 773, 739, 698 cm^{-1}. ^1H NMR (400 MHz, $CDCl_3$): δ = 0.85–0.97 (m, 1H), 1.38 (s, 9H), 1.47–1.54 (m, 1H), 1.59–1.66 (m, 3H), 1.81–1.94 (m, 2H), 2.20 (s, 3H), 2.21 (s, 3H), 2.31 (t, J = 7.4 Hz, 1H), 2.38 (t, J = 7.0 Hz, 1H), 2.72 (br s, 2H), 3.02–3.06 (m, 2H), 3.11–3.27 (m, 2H), 3.45 (s, 2H), 7.17–7.26 (m, 5H). ^{13}C NMR (100 MHz, $CDCl_3$): δ = 24.81, 28.32, 28.52, 35.61, 36.03, 45.43, 45.57, 45.67, 50.84, 51.25, 53.93, 54.13, 56.81, 57.51, 57.70, 58.06, 63.50, 79.20, 79.28, 126.82, 126.86, 128.06, 129.06, 129.13, 138.09, 138.20, 155.55. HRMS (ESI+): *m/z* calcd for $C_{22}H_{38}N_3O_2$ 376.2964; found 376.2972. HPLC purity, 96% at 254 nm (method B, t_R = 7.60 min).

(±)-Tert-butyl ((1-benzylpiperidin-3-yl)methyl)(3-(dimethylamino)propyl)carbamate (13)

Synthesized from crude (±)-N^1-((1-benzylpiperidin-3-yl)methyl)-N^3,N^3-dimethylpropane-1,3-diamine (**9**) (3.397 g, 11.736 mmol) via general procedure 4. Purified by flash column chromatography using CH_2Cl_2/MeOH/Et_3N (130:10:1, v/v) as the eluent to produce 1.859 g **13** as a colorless oil (41% yield). IR (ATR): 2974, 2931, 2764, 1685, 1462, 1421, 1360, 1243, 1152, 1110, 1067, 1022, 887, 866, 771, 742, 695 cm^{-1}. ^1H NMR (400 MHz, $CDCl_3$): δ = 0.83–0.96 (m, 1 H), 1.40 (s, 9 H), 1.45–1.53 (m, 1 H), 1.58–1.64 (m, 3 H), 1.80–1.92 (m, 2 H), 2.18 (s, 3 H), 2.24 (s, 3 H), 2.31–2.41 (m, 4 H), 2.74 (bs, 2H), 3.01–3.07 (m, 2H), 3.14–3.30 (m, 2H), 3.43 (s, 2H), 7.18–7.25 (m, 5H). ^{13}C NMR (100 MHz, $CDCl_3$): δ = 24.80, 25.22, 25.45 28.31, 28.54, 35.60, 36.06, 45.47, 45.61, 45.64, 50.88, 51.29, 53.92, 54.16, 56.84, 57.50, 57.96, 58.10, 63.52, 79.23, 79.31, 126.80, 126.90, 128.09, 129.07, 129.16, 138.10, 138.22, 155.59. HRMS (ESI+):

m/z calcd for $C_{23}H_{40}N_3O_2$ 390.3121; found 390.3130. HPLC purity, 97% at 254 nm (method B, t_R = 7.76 min).

(±)-Tert-butyl (2-(dimethylamino)ethyl)(piperidin-3-ylmethyl)carbamate (14)

Synthesized from (±)-*tert*-butyl ((1-benzylpiperidin-3-yl)methyl)(2-(dimethylamino)ethyl)carbamate (**12**) (3.190 g, 8.494 mmol) via general procedure 5, to produce 2.410 g crude **14** as a pale yellow oil (99% yield). This product was used in the next step without further purification. HRMS (ESI+): *m/z* calcd for $C_{15}H_{32}N_3O_2$ 286.2495; found 286.2487.

(±)-Tert-butyl (3-(dimethylamino)propyl)(piperidin-3-ylmethyl)carbamate (15)

Synthesized from (±)-N^1-((1-benzylpiperidin-3-yl)methyl)-N^3,N^3-dimethylpropane-1,3-diamine (**13**) (1.747 g, 4.484 mmol) via general procedure 5, to produce 1.318 g crude **15** as a colorless oil (98% yield). This product was used in the next step without further purification. HRMS (ESI+): *m/z* calcd for $C_{16}H_{34}N_3O_2$ 300.2651; found 300.2655.

(±)-Tert-butyl ((1-(2,3-dihydro-1H-inden-2-yl)piperidin-3-yl)methyl)(2-(dimethylamino)ethyl)carbamate (16)

Synthesized from (±)-*tert*-butyl (2-(dimethylamino)ethyl)(piperidin-3-ylmethyl)carbamate (**14**) (1.920 g, 6.727 mmol) via general procedure 6. Purified by flash column chromatography using CH_2Cl_2/MeOH (9:1, v/v) as the eluent to produce 1.870 g **16** as a pale golden oil (69% yield). R_f = 0.11 (CH_2Cl_2/MeOH, 9:1, v/v). IR (ATR): 2934, 2766, 1690, 1461, 1416, 1390, 1365, 1249, 1156, 1099, 1023, 937, 888, 863, 771, 742 cm^{-1}. ^1H NMR (400 MHz, $CDCl_3$): δ = 0.87–1.01 (m, 1H), 1.44 (s, 9H), 1.60–1.83 (m, 4H), 1.92–1.97 (m, 2H), 2.24 (s, 6H), 2.38–2.46 (m, 2H), 2.86–2.96 (m, 4H), 3.01–3.15 (m, 5H), 3.24 (t, J = 7.2 Hz, 1H), 3.30 (t, J = 7.4 Hz, 1H), 7.08–7.14 (m,

4H). ^{13}C NMR (100 MHz, $CDCl_3$): δ = 24.80, 24.89, 28.33, 28.68, 35.69, 36.02, 36.81, 37.02, 45.43, 45.55, 45.64, 50.88, 51.45, 52.11, 56.16, 56.43, 56.82, 57.52, 67.19, 79.33, 124.25, 126.27, 141.35, 141.39, 155.51, 155.62. HRMS (ESI+): *m/z* calcd for $C_{14}H_{40}N_3O_2$ 402.3121; found 402.3115. HPLC purity, 98% at 254 nm (method B, t_R = 8.46 min).

(±)-Tert-butyl ((1-(2,3-dihydro-1H-inden-2-yl)piperidin-3-yl)methyl)(3-(dimethylamino)propyl)carbamate (17)

Synthesized from crude (±)-*tert*-butyl (3-(dimethylamino)propyl)(piperidin-3-ylmethyl)carbamate (**15**) (1.318 g, 4.401 mmol) via general procedure 6. Purified by flash column chromatography using CH_2Cl_2/MeOH/Et_3N (100:10:1, v/v) as the eluent to produce 0.866 g **17** as a slightly purple oil (47% yield). R_f = 0.27 (CH_2Cl_2/MeOH/Et_3N, 100:10:1, v/v). IR (ATR): 2932, 2761, 1689, 1416, 1364, 1156, 1232, 1127, 866, 742 cm^{-1}. ^{1}H NMR (400 MHz, $CDCl_3$): δ = 0.89–1.02 (m, 1 H), 1.45 (s, 9 H), 1.68–1.75 (m, 4 H), 1.90–1.99 (m, 4 H), 2.21–2.26 (m, 8 H), 2.85–2.96 (m, 4 H), 3.02–3.24 (m, 7 H), 7.11–7.18 (m, 4 H). ^{13}C NMR (100 MHz, $CDCl_3$): δ = 24.97, 26.03, 26.60, 28.35, 28.38, 28.53, 28.72, 35.62, 35.93, 36.95, 37.19, 45.34, 45.38, 45.51, 45.66, 50.53, 50.95, 52.20, 56.25, 56.44, 56.98, 57.10, 67.21, 79.14, 124.25, 126.23, 141.49, 155.56, 155.77. HRMS (ESI+): *m/z* calcd for $C_{25}H_{42}N_3O_2$ 416.3277; found 416.3270. HPLC purity, 96% at 254 nm (method B, t_R = 8.63 min).

(±)-N^1-((1-(2,3-Dihydro-1H-inden-2-yl)piperidin-3-yl)methyl)-N^2,N^2-dimethylethane-1,2-diamine tris(2,2,2-trifluoroacetate) (18)

Synthesized from (±)-*tert*-butyl ((1-(2,3-dihydro-1*H*-inden-2-yl)piperidin-3-yl)methyl)(2-(dimethylamino)ethyl)carbamate (**16**) (1.870 g, 4.656 mmol) via general procedure 7, to produce 2.950 g crude **18** as white solid (98% yield). This product was used in the next step without

further purification. R_f = 0.08 (CH_2Cl_2/MeOH, 9:1, v/v). HRMS (ESI+): *m/z* calcd for $C_{19}H_{32}N_3$ 302.2596; found 302.2591.

(±)-N^1-((1-(2,3-Dihydro-1H-inden-2-yl)piperidin-3-yl)methyl)-N^3,N^3-dimethylpropane-1,3-diamine tri(2,2,2-trifluoroacetate) (19)

Synthesized from (±)-*tert*-butyl ((1-(2,3-dihydro-1*H*-inden-2-yl)piperidin-3-yl)methyl)(3-(dimethylamino)propyl)carbamate (**17**) (0.816 g, 1.963 mmol) via general procedure 7, to produce 1.223 g crude **19** as a white solid (95% yield). This product was used in the next step without further purification. HRMS (ESI+): *m/z* calcd for $C_{20}H_{34}N_3$ 316.2753; found 316.2759.

(±)-N-((1-(2,3-Dihydro-1H-inden-2-yl)piperidin-3-yl)methyl)-N-(3-(dimethylamino)propyl)-2-naphthamide (20)

Synthesized from crude (±)-N^1-((1-(2,3-dihydro-1*H*-inden-2-yl)piperidin-3-yl)methyl)-N^3,N^3-dimethylpropane-1,3-diamine tri(2,2,2-trifluoroacetate) (**19**) (0.164 g, 0.249 mmol) and 2-naphthoyl chloride via general procedure 1. Purified by flash column chromatography using CH_2Cl_2/MeOH/Et_3N (100:10:1, v/v) as the eluent to produce 0.100 g **20** as a slightly golden-yellow oil (85% yield). R_f = 0.23 (CH_2Cl_2/MeOH, 1:1, v/v). IR (ATR): 2936, 2767, 1686, 1623, 1460, 1198, 1135, 1038, 824, 734, 719 cm^{-1}. ^1H NMR (400 MHz, DMSO-d6, 80 °C): δ = 0.93 (bs, 1 H), 1.42–1.53 (m, 1 H), 1.57–1.69 (m, 2 H), 1.84 (bs, 1 H), 2.01–2.11 (m, 7 H), 2.52–2.63 (m, 2 H), 2.72–2.86 (m, 4 H), 2.98–3.24 (m, 6 H), 3.37–3.44 (m, 4 H), 7.11–7.22 (m, 4 H), 7.43–7.45 (m, 1 H), 7.54–7.61 (m, 2 H), 7.89 (s, 1 H), 7.93–7.99 (m, 3 H). ^{13}C NMR (100 MHz, $CDCl_3$): δ = 24.82, 24.89, 25.22, 25.31, 28.52, 28.65, 29.66, 35.39, 36.89, 43.06, 45.57, 45.69,

47.25, 48.19, 51.93, 53.52, 55.64, 56.22, 56.75, 57.70, 66.96, 67.17, 124.07, 124.32, 124.36, 125.99, 126.34, 126.59, 126.84, 127.76, 128.25, 128.23, 132.62, 133.37, 134.21, 141.46, 172.18, 172.39. HRMS (ESI+): *m/z* calcd for $C_{31}H_{40}N_3O$ 470.3171; found 470.3180. HPLC purity, 97% at 254 nm (method B, t_R = 9.28 min).

2-((Tert-butoxycarbonyl)(methyl)amino)ethyl methanesulfonate (22)

To a 100-mL round-bottomed flask equipped with a stirring bar, *tert*-butyl (2-hydroxyethyl)(methyl)carbamate (**21**) (2.000 g, 11.414 mmol, 1.0 equiv.) and DCM (50 mL) were added and cooled on an ice bath (0 °C). The resulting solution was stirred, and Et_3N (3.165 mL, 22.828 mmol, 2.0 equiv.) and methanesulfonyl chloride (1.105 mL, 14.268 mmol, 1.25 equiv.) were added drop-wise. The reaction mixture was stirred at room temperature for 2 h. The reaction mixture was transferred into a separating funnel, washed with water (2 × 50 mL), saturated brine solution (50 mL), dried over anhydrous Na_2SO_4, and evaporated to obtain 2.810 g **22** as a colorless oil (97% yield). This product was used in the next step without further purification. R_f = 0.43 (EtOAc/*n*-hex, 1:1, v/v).

(±)-Tert-butyl (2-(N-((1-(2,3-dihydro-1H-inden-2-yl)piperidin-3-yl)methyl)-2-naphthamido)ethyl)(methyl)carbamate (24)

To a 50-mL round-bottomed flask equipped with a stirring bar, **23** (1.320 g, 3.433 mmol, 1.0 equiv.) was added and purged under a stream of argon for 15 min, and then anhydrous DMF (15 mL) and Et_3N (1.903 mL, 13.732 mmol, 4.0 equiv.) were added. The resulting solution was cooled on an ice bath (0 °C), and NaH (60% dispersion on mineral oil, 0.412 g, 10.299 mmol, 3.0 equiv.) was added in small portions. After 2 h stirring at room temperature, **22** (2.609 g, 10.299 mmol, 3.0 equiv.) was added drop-wise. The reaction mixture was stirred at 50 °C for 72 h. The

reaction was quenched by adding saturated aqueous $NaHCO_3$ solution (5 mL), then the solvent was evaporated under reduced pressure. The residue was dissolved in DCM (80 mL), transferred into a separating funnel, washed with saturated aqueous $NaHCO_3$ solution (50 mL), water (2 × 50 mL), followed by saturated brine solution, dried over anhydrous Na_2SO_4, and evaporated. The crude product was purified by flash column chromatography using DCM/MeOH (30:1, v/v) to produce 0.952 g **24** as a colorless oil (51% yield). R_f = 0.23 (DCM/MeOH, 30:1, v/v). ^{1}H-NMR (400 MHz, $CDCl_3$): δ = 0.57–0.65 (m, 0.6 H), 1.13–1.18 (m, 0.4 H), 1.31–1.59 (m, 11 H), 1.93–2.26 (m, 3 H), 2.36–2.46 (m, 1 H), 2.81–3.82 (m, 16 H), 7.13–7.19 (m, 4 H), 7.41–7.45 (m, 1 H), 7.52–7.53 (m, 2 H), 7.83–7.92 (m, 4 H).

(±)-N-((1-(2,3-Dihydro-1H-inden-2-yl)piperidin-3-yl)methyl)-N-(2-(methylamino)ethyl)-2-naphthamide dihydrochloride (25 dichloride)

To a 100-mL round-bottomed flask equipped with a stirring bar, **24** (0.075 g, 0.138 mmol, 1.0 equiv.) and EtOH (40 mL) were added followed by concentrated HCl (37%, 0.570 mL, 6.900 mmol, 50.0 equiv.). The resulting solution was stirred at 50 °C for 16 h, and the solvent was evaporated under reduced pressure. The crude product was purified by reversed phase column chromatography (Isolera Biotage system, SNAP KP-C18-HS, 12 g column) using water/MeCN (80:20, v/v) as an eluent. The fractions containing compound **25 dichloride** were pooled, and the MeCN evaporated. The residue was frozen and lyophilized to produce 0.050 g **25 dichloride** as a white solid (70% yield). mp 137–140 °C. IR (ATR): 3422, 1942, 2689, 1662, 1654, 1479, 1458, 1430, 1384, 1313, 1288, 1236, 1196, 1133, 1026, 869, 827, 777, 755 cm^{-1}. ^{1}H-NMR (400 MHz, MeOD): δ = 0.92–1.00 (m, 0.6 H), 1.81–2.16 (m, 3 H), 2.33–2.65 (m, 2.4 H), 2.76–2.90 (m, 3 H), 3.19–3.34 (m, 4 H), 3.40–3.60 (m, 6 H), 3.75–4.26 (m, 4 H), 7.21–7.30 (m, 4 H), 7.53–7.55 (m, 1

H), 7.60–7.66 (m, 2 H), 7.96–8.06 (m, 4 H). HRMS (ESI+): *m/z* calcd for $C_{29}H_{36}N_3O$ $[M+H]^+$ 442.2858; found 442.2854. HPLC purity, 96% at 254 nm (method E, t_R = 10.22 min).

Experimental Properties of the Most Potent Class I-VII Inhibitors 26-32

(±)-6-Bromo-N-((1-(2,3-dihydro-1H-inden-2-yl)piperidin-3-yl)methyl)-N-(2-methoxyethyl)-2-naphthamide (26)

Synthesized from (±)-*N*-((1-(2,3-dihydro-1*H*-inden-2-yl)piperidin-3-yl)methyl)-2-methoxyethan-1-amine di(2,2,2-trifluoroacetate)[35] (**33**) (0.151 g, 0.292 mmol) and 6-bromo-2-naphthoic acid via general procedure 2. Purified by flash column chromatography using CH_2Cl_2/MeOH (20/1, v/v) as the eluent to produce 0.132 g **26** as a colorless oil (87% yield). R_f = 0.50 (CH_2Cl_2/MeOH, 20/1, v/v). IR (ATR): 2929, 1623, 1470, 1348, 1177, 1115, 1063, 877, 742 cm^{-1}. ^1H NMR (400 MHz, $CDCl_3$): δ = 0.90 (bd, J = 217.3 Hz, 1 H), 1.66 (bs, 4 H), 1.81 (bs, 1 H), 1.96–2.16 (m, 2 H), 2.82 (bs, 2 H), 2.98–3.11 (m, 4 H), 3.23 (bs, 2 H), 3.31 (bs, 1 H), 3.38 (bs, 1 H), 3.42 (bs, 1 H), 3.48 (bs, 1 H), 3.55 (1 H, bs), 3.72 (bs, 2 H), 7.12–7.19 (m, 4 H), 7.43–7.50 (m, 1 H), 7.60 (dd, J_1 = 8.7, J_2 = 2.0 Hz, 1 H), 7.71–7.83 (m, 3 H), 8.03 (d, J = 1.8 Hz, 1 H). ^{13}C NMR (100 MHz, $CDCl_3$): δ = 24.65, 24.89, 28.35, 28.54, 35.05, 35.28, 36.80, 44.92, 48.06, 48.59, 51.81, 51.91, 54.12, 55.43, 56.04, 58.82, 66.84, 67.05, 70.04, 70.46, 120.89, 124.25, 125.38, 126.30, 127.29, 129.78, 129.80, 129.99, 130.99, 134.24, 134.55, 141.37, 171.73, 172.07. HRMS (ESI+): *m/z* calcd for $C_{29}H_{34}N_2O_2$ 521.1804; found 521.1811. HPLC purity, 97% at 254 nm (method A, t_R = 13.48 min).

(±)-N-((1-(2,3-Dihydro-1H-inden-2-yl)piperidin-3-yl)methyl)-1-naphthamide (27)

Synthesized from (±)-(1-(2,3-dihydro-1*H*-inden-2-yl)piperidin-3-yl)methanamine di(2,2,2-trifluoroacetate)[71] (**34**) (0.101 g, 0.220 mmol) and 1-naphthoyl chloride via general procedure 1.

Purified by precipitation from a solution in EtOAc by adding *n*-hexante to produce 0.080 g **27** as a slightly pink solid (94% yield). R_f = 0.40 (CH_2Cl_2/MeOH, 10:1, v/v). IR (ATR): 3276, 2929, 2847, 1637, 1537, 1302, 1127, 1021, 777, 741 cm^{-1}. ^1H NMR (400 MHz, $CDCl_3$): δ = 1.13–1.23 (m, 1 H), 1.66–1.73 (m, 1 H), 1.93 (bs, 2 H), 2.05 (d, J = 5.7 Hz, 2 H), 2.13 (t, J = 10.7 Hz, 2 H), 2.91–2.98 (m, 3 H), 3.06–3.15 (m, 3 H), 3.21–3.29 (m, 1 H), 3.44–3.57 (m, 2 H), 6.31 (bs, 1 H), 7.12–7.18 (m, 4 H), 7.46 (dd, J_1 = 8.3, J_2 = 7.0 Hz, 1 H), 7.51–7.57 (m, 2 H), 7.60 (dd, J_1 = 7.0, J_2 = 1.3 Hz, 1 H), 7.86–7.89 (m, 1 H), 7.92 (d, J = 8.3 Hz, 1 H), 8.28–8.33 (m, 1 H). ^{13}C NMR (100 MHz, $CDCl_3$): δ = 24.38, 28.34, 36.25, 36.60, 36.77, 43.46, 51.86, 55.80, 66.96, 124.21, 124.56, 124.64, 125.27, 126.22, 126.30, 126.85, 128.13, 129.69, 130.26, 133.47, 134.51, 141.13, 141.16, 169.60. HRMS (ESI+): *m/z* calcd for $C_{26}H_{29}N_2O$ 385.2280; found 385.2288. HPLC purity, 96% at 254 nm (method A, t_R = 9.63 min).

(±)-N-((1-Benzylpiperidin-3-yl)methyl)-N-(2-methoxyethyl)-2-naphthamide (28)

Synthesized from (±)-*N*-((1-benzylpiperidin-3-yl)methyl)-2-methoxyethan-1-amine[45] (**35**) (0.094 g, 0.358 mmol) and 2-naphthoyl chloride via general procedure 1. Purified by flash column chromatography using CH_2Cl_2/MeOH (20:1, v/v) as the eluent to produce 0.134 g **28** as a colorless oil (90% yield). IR (ATR): 2929, 2809, 1624, 1421, 1194, 1115, 1070, 822, 742, 699 cm^{-1}. ^1H NMR (400 MHz, $CDCl_3$): δ = 0.90 (dd, J_1 = 208.8, J_2 = 8.9 Hz, 1 H), 1.42–1.49 (m, 1 H), 1.76 (bs, 4 H), 1.92 (bs, 1 H), 2.10 (bs, 1 H), 2.64 (bs, 1 H), 2.86 (bs, 1 H), 3.19–3.32 (m, 3 H), 3.40 (bs, 3 H), 3.48–3.60 (m, 2 H), 3.69–3.79 (m, 2 H), 7.20 (bs, 1 H), 7.27–7.45 (m, 5 H), 7.53 (bs, 2 H), 7.71–7.90 (m, 4 H). ^{13}C NMR (100 MHz, $CDCl_3$): δ = 24.49, 24.76, 28.06, 28.42, 34.73, 35.15, 44.81, 48.04, 48.55, 53.47, 53.90, 54.37, 57.24, 58.76, 63.28, 63.33, 63.39, 70.22, 70.44, 124.21, 124.35, 126.02, 126.36, 126.46, 126.70, 126.92, 127.69, 128.09, 128.14, 128.21, 129.04, 129.25, 132.56, 133.24, 134.17, 137.77, 138.21, 172.14, 172.37. R_f = 0.41

(CH_2Cl_2/MeOH, 10:1, v/v). HRMS (ESI+): *m/z* calcd for $C_{27}H_{33}N_2O_2$ 417.2542; found 417.2530. HPLC purity, 98% at 254 nm (method A, t_R = 10.92 min).

(±)-N-((1-Benzylpiperidin-3-yl)methyl)-2-naphthamide (29)

Synthesized from (±)-(1-benzylpiperidin-3-yl)methanamine[45] (**36**) (0.050 g, 0.245 mmol) and 2-naphthoyl chloride via general procedure 1. Purified by flash column chromatography using CH_2Cl_2/MeOH (13:1, v/v) as the eluent to produce 0.056 g **7** as a slightly brown oil (64% yield). R_f = 0.34 (CH_2Cl_2/MeOH, 10:1, v/v). IR (ATR): 3325, 2937, 1625, 1532, 1304, 1237, 1071, 823, 761, 698 cm-1. ^{1}H NMR (400 MHz, $CDCl_3$): δ = 1.20–1.28 (m, 1 H), 1.56–1.66 (m, 1 H), 1.72–1.82 (m, 1 H), 1.85 (bs, 1 H), 1.95–2.05 (m, 1 H), 2.11 (bs, 1 H), 2.24 (bs, 1 H), 2.64–2.67 (m, 1 H), 2.78 (d, J = 10.3 Hz, 1 H), 3.42–3.57 (m, 4 H), 6.69 (bs, 1 H), 7.21–7.25 (m, 1 H), 7.27–7.32 (m, 4 H), 7.51–7.58 (m, 2 H), 7.75 (dd, J_1 = 8.5 Hz, J_2= 1.8 Hz, 1 H), 7.86–7.90 (m, 3 H), 8.20 (s, 1 H). ^{13}C NMR (100 MHz, $CDCl_3$): δ = 24.25, 28.39, 35.66, 43.93, 54.07, 57.52, 63.45, 123.58, 126.61, 127.05, 127.22, 127.48, 127.67, 128.21, 128.33, 128.88, 129.16, 131.94, 132.55, 134.59, 138.04, 167.62. HRMS (ESI+): *m/z* calcd for $C_{24}H_{27}N_2O$ 359.2123; found 359.2121. HPLC purity, 98% at 254 nm (method A, t_R = 9.84 min).

(±)-N-((1-(Benzo[d]thiazol-2-ylmethyl)piperidin-3-yl)methyl)-2-naphthamide (30)

Synthesized from crude (±)-(1-(benzo[*d*]thiazol-2-ylmethyl)piperidin-3-yl)methanamine di(2,2,2-trifluoroacetate)[71] (**37**) (0.080 g, 0.163 mmol) and 2-naphthoyl chloride via general procedure 2. Purified by flash column chromatography using EtOAc/*n*-hex (1:1, v/v) as the eluent and then precipitated from a solution in CH_2Cl_2 by adding *n*-hex, to produce 0.028 g **30** as a white solid (41% yield). R_f = 0.16 (EtOAc/*n*-hex, 1:1, v/v). IR (KBr): 3338, 2934, 1637, 1541, 1441, 1281, 1239, 1171, 865, 826, 780, 758, 728 cm^{-1}. ^{1}H NMR (400 MHz, $CDCl_3$): δ = 1.23–1.29 (m, 1 H),

1.62–1.69 (m, 1 H), 1.79–1.86 (m, 2 H), 2.07(br s, 1 H), 2.30 (t, J = 8.2 Hz, 1 H), 2.42 (t, J = 8.6 Hz, 1 H), 2.79–2.81 (m, 1 H), 2.90 (d, J = 10.4 Hz, 1 H), 3.51 (bs, 2 H), 3.89–3.98 (m, 2 H), 6.57 (bs, 1 H), 7.34 (t, J = 7.2 Hz, 1 H), 7.44 (t, J = 8.2 Hz, 1 H), 7.49–7.55 (m, 2 H), 7.74–7.84 (m, 5 H), 7.94–7.96 (m, 1 H), 8.18 (s, 1 H). ^{13}C NMR (100 MHz, $CDCl_3$): δ = 24.27, 27.85, 36.15, 43.32, 54.67, 57.83, 60.79, 121.70, 122.74, 123.51, 124.85, 125.82, 126.65, 127.19, 127.53, 127.66, 128.39, 128.85, 131.85, 132.51, 134.60, 135.22, 153.22, 167.65, 172.68. HRMS (ESI+): m/z calcd for $C_{25}H_{26}N_3OS$ 416.1797; found 416.1787. HPLC purity, 97% at 254 nm (method A, t_R = 9.63 min).

(±)-N-((1-(2,3-Dihydro-1H-inden-2-yl)piperidin-3-yl)methyl)-N-(3-methoxypropyl)-2-naphthamide (31)

Synthesized from crude (±)-*N*-((1-(2,3-dihydro-1*H*-inden-2-yl)piperidin-3-yl)methyl)-3-methoxypropan-1-amine di(2,2,2-trifluoroacetate) (**38**) (0.200 g, 0.377 mmol) and 2-naphthoyl chloride via general procedure 1. Purified by flash column chromatography using CH_2Cl_2/MeOH (20:1, v/v) as the eluent to produce 0.168 g **31** as a slightly brown oil (98% yield). R_f = 0.45 (CH_2Cl_2/MeOH, 10:1, v/v). IR (ATR): 2929, 1624, 1477, 1422, 1227, 1198, 1114, 863, 822, 743 cm^{-1}. ^{1}H NMR (400 MHz, $CDCl_3$): δ = 0.90 (bdd, J_1 = 218.0, J_2 = 9.8 Hz, 1 H), 1.71 (bs, 5 H), 2.01–2.23 (m, 3 H), 2.84 (bs, 2 H), 2.96–3.18 (m, 7 H), 3.25 (bs, 1 H), 3.39 (bs, 3 H), 3.53 (bs, 2 H), 3.65 (bs, 1 H), 7.13–7.20 (m, 4 H), 7.39–7.45 (m, 1 H), 7.50–7.56 (m, 2 H), 7.80–7.88 (m, 4 H). ^{13}C NMR (100 MHz, $CDCl_3$): δ = 24.51, 27.31, 28.17, 28.33, 34.66, 35.02, 36.61, 42.43, 46.13, 47.35, 51.60, 51.72, 53.12, 53.22, 55.27, 55.79, 58.13, 58.36, 66.64, 66.83, 68.99, 70.12, 123.72, 124.06, 125.71, 126.12, 126.35, 126.57, 127.51, 127.98, 128.02, 132.39, 133.08, 134.01, 141.10, 141.16, 171.80, 171.99. HRMS (ESI+): *m/z* calcd for $C_{30}H_{37}N_2O_2$ 457.2855; found 457.2851. HPLC purity, 98% at 254 nm (method A, t_R = 11.48 min).

N-((1-Benzylpiperidin-4-yl)methyl)-N-(2-methoxyethyl)-2-naphthamide (32)

Synthesized from crude *N*-((1-benzylpiperidin-4-yl)methyl)-2-methoxyethan-1-amine[45] (**39**) (0.145 g, 0.553 mmol) and 2-naphthoyl chloride via general procedure 1. Purified by flash column chromatography using CH_2Cl_2/MeOH (20/1, v/v) as the eluent to produce 0.227 g **32** as a colorless oil (99% yield). R_f = 0.47 (CH_2Cl_2/MeOH, 10/1, v/v). IR (ATR): 2925, 2812, 1633, 1422, 1284, 1119, 1073, 974, 832, 738, 699 cm^{-1}. ^1H NMR (400 MHz, $CDCl_3$): δ = 0.88–0.98 (m, 1 H), 1.40–1.53 (m, 2 H), 1.76–1.92 (m, 4 H), 1.99–2.05 (m, 1 H), 2.79 (bd, J = 9.7 Hz, 1 H), 2.95 (bs, 1 H), 3.22 (bs, 1 H), 3.33–3.54 (m, 7 H), 3.73 (bs, 2 H), 7.22–7.25 (m, 2 H), 7.27–7.33 (m, 3 H), 7.41–7.48 (m, 1 H), 7.50–7.53 (m, 2 H), 7.81–7.86 (m, 4 H). ^{13}C NMR (100 MHz, $CDCl_3$): δ = 29.48, 29.90, 34.15, 34.62, 44.71, 49.35, 50.71, 53.11, 55.70, 58.76, 63.12, 70.29, 70.55, 124.25, 126.20, 126.32, 126.43, 126.69, 126.80, 127.62. 127.98, 128.11, 128.14, 129.05, 132.51, 133.20, 133.95, 134.21, 137.99, 138.10, 172.22, 172.28. HRMS (ESI+): *m/z* calcd for $C_{27}H_{33}N_2O_2$ 417.2542; found 417.2545. HPLC purity, 97% at 254 nm (method A, t_R = 10.86 min).

Materials and Methods

The rats used in the rat brain slice experiments and the *in vivo* blood plasma–brain distribution assays were handled according to the European Community Council Directive of 23 November 1986 (86/609/EEC), and the National Veterinary Institute Guide for the Care and Use of Laboratory Animals. The experimental design was evaluated by the National Ethical Committee for Animal Experimentation, and was approved by the Veterinary Administration of the Republic of Slovenia. The maintenance and treatment of the mice used in the *in vivo* activity and *in vivo* safety assays were carried out in full accordance with the guidelines issued by the Local Ethics

Committee of the Jagiellonian University in Krakow (ZI/862/2013). All efforts were made to minimize both the number of animals used, and their suffering.

Separation of Compound 3 by Semi-Preparative Reverse-Phase Chiral HPLC

The resolution of compound **3** was accomplished by 35 runs of method C. Eluates corresponding to the two chromatographic peaks were pooled and evaporated to about 5 mL, and then transferred to a 50-mL separating funnel. Water (6 mL) and saturated aqueous $NaHCO_3$ solution (6 mL) were added and extracted with CH_2CL_2 (20 mL). The organic phase was dried over anhydrous Na_2SO_4, and evaporated, to produce 24.5 mg of the first-eluted enantiomer as a colorless oil, and 8.5 mg of the second-eluted enantiomer as a colorless oil. Analytical reversed-phase chiral HPLC analysis (method D, 254 nm) of both enantiomers gave an enantiomeric excess (e.e.) of 99%. The specific rotation of the first-eluted enantiomer was $[\alpha]_D^{23}$ –23.28 (*c* 0.251, $CHCl_3$), while the specific rotation of the second-eluted enantiomer was $[\alpha]_D^{23}$ +23.10 (*c* 0.247, $CHCl_3$). The analytical reversed-phase chiral HPLC retention times were (method D, 254 nm): **(–)-3**, 38.55 min; **(+)-3**, 38.85 min.

***In Vitro* Cholinesterase Inhibitory Activity and IC_{50} Calculations**

Ellman's method was used to evaluate the inhibitory activities of the synthesized compounds against the cholinesterases.[46] Butyrylthiocholine and acetylthiocholine iodides and 5,5′-dithiobis (2-nitrobenzoic acid) (Ellman's reagent, DTNB) were purchased from Sigma-Aldrich (Steinheim, Germany). The murine (m)AChE and recombinant huBChE (4.6 mg/mL, 10 mM MES buffer, pH 6.5) were kindly donated by Florian Nachon (IBS, Grenoble).

Inhibitory activity screening against the cholinesterases

The reactions were carried out in a final volume of 300 μL of 0.1 M phosphate-buffered solution, pH 8.0, containing 333 μM DTNB, 5×10^{-4} M butyrylthiocholine or acetylthiocholine iodides and 1×10^{-9} M or 5×10^{-11} M huBChE or mAChE, respectively. The formation of the yellow 5-thio-2-nitrobenzoate anion as a result of the reaction of DTNB with the thiocholines was monitored for 1 min, as change in absorbance at 412 nm, using a 96-well microplate reader (Synergy H4; BioTek Instruments, Inc., USA). To determine the blank (b), phosphate-buffered solution replaced the enzyme solution. The initial velocity (v_0) was calculated from the slope of the linear trend obtained, with each measurement carried out in triplicate. For the initial screening, stock solutions of the test compounds (1 mM) were prepared in DMSO and studied at a 10 μM final well concentration. The content of organic solvent (DMSO) was always 1%. The reactions were started by the addition of the substrate to the enzyme and inhibitor that had been preincubated for 300 s, to allow complete equilibration of the enzyme–inhibitor complexes. Tacrine was used as a standard inhibitor. The initial velocities in the presence of the test compounds (v_i) were calculated. The inhibitory potencies are expressed as the residual activities [RA = (v_i – b) / (v_o – b)]. For the IC_{50} measurements, eight different concentrations of each compound were used to obtain enzyme activities of between 5% and 90%. Each concentration was tested in triplicate. The IC_{50} values were obtained by plotting the residual enzyme activities against the applied inhibitor concentrations, with the experimental data fitted to Equation (1):

$$Y = \text{Bottom} + (\text{Top} - \text{Bottom}) / (1+10\hat{}((\text{Log}IC_{50} - X) \times \text{HillSlope})) \qquad (1),$$

where X is the logarithm of the inhibitor concentration, and Y is the residual activity. For the fitting procedure, the Gnuplot software and an in-house python script were used.

HuBChE Inhibition Kinetics Studies

The mode of action of huBChE inhibition by pure enantiomers of compound **3** was determined as previously described.[29,35] Briefly, the time-course of yellow color formation was followed on a Bio-logic SFM-2000 stopped-flow apparatus and a Perkin Elmer Lambda 45 UV/Vis spectrometer at 25 °C. The buffer solutions of all components were mixed in cuvette, and the resulting solution contained 47 μM BTCI, 1 mM DTNB, 3.4 nM huBChE, 3.5 nM test compound **3** (each as pure enantiomers or a racemic mixture), and 0.007 M DMSO (i.e., 0.05%). The absorbance was followed at 412 nm immediately using Perkin Elmer Lambda 45 UV/Vis spectrometer. The progress curves obtained were analyzed simultaneously, with the ENZO application,[49] which can derive and numerically solve a system of differential equations, and fit their coefficients. Several reaction mechanisms were tested. The simplest one for the reproduction of the progress curves in the absence and presence of (+)-**3** and (–)-**3** was chosen, and the corresponding inhibition constants were determined. The results file can be accessed by loading the ENZO project ID 170501222, selecting the "Set Parameters" tab, and pressing "Start". The experiment was also performed with three different concentrations of **(+)-3** in duplicate using stopped-flow apparatus. The two buffer solutions were prepared as one that contained the substrate butyrylthiocholine iodide, the reagent DTNB, and the test compound **(+)-3** and the other that contained the huBChE. The buffer solutions were injected into a mixing chamber using syringes. The resulting solution contained 50.4 μM butyrylthiocholine iodide, 1 mM DTNB, 1.07 nM huBChE, test compound **(+)-3** (at concentrations 0.4 nM. 0.8 nM and 2.0 nM), and 0.007 M DMSO (i.e., 0.05%). The absorbance was followed at 412 nm immediately, and until the change reached zero. The progress curves obtained were analyzed as described above.

Crystallization, and Data Collection and Processing

Human BChE was expressed in the CHO cell line, purified and concentrated to 6 mg/mL, as previously described.[72] Co-crystallization was performed to obtain the crystal structure of compound **3** bound to huBChE. Briefly, 500 μM aqueous solution (1% DMSO) of compound **3** was incubated with 90 μM huBChE solution for 3 h. Co-crystals grew at room temperature within approximately 3 weeks using the hanging-drop vapor diffusion method. The mother liquor solution was 0.1 M Tris, pH 8.1, 2.3 M ammonium sulfate. Prior to data collection, the crystals were cryoprotected by a short soak in a mother liquor solution complemented with 18% glycerol and compound **3** (500 μM), before being flash-cooled directly in the N_2 gas stream at 100 K at the beamline. The data were collected at the beamline ID30A3 of the European Synchrotron Radiation Facility (Grenoble, France) using a wavelength of 0. 9679 Å. Data were indexed and integrated using XDS,[73] and were scaled and merged with XSCALE. The structure was solved using the molecular replacement method, using PHASER[74] and a huBChE model (PDB ID 1POM) as a search model, depleted of all ligands, and with the sugars removed. Reciprocal-space refinement was performed using Phenix,[75] which was intersperced with cycles of model building with Coot.[76] Following an, initial rigid-body refinement, each reciprocal-space refinement cycle consisted of energy minimization and individual isotropic temperature factor refinement. The ligand topology was generated with the PRODRG server.[77] Data collection and refinement statistics are presented in Supporting Table S7. The coordinates and structure factors have been deposited in the Protein Data Bank under accession ID 5NN0.

Thermodynamic Analysis of Binding

The time course of BTCI hydrolysis by hBChE in the absence and presence of compounds **(+)-1** and **(+)-3** was measured at three temperatures [293 K, 298 K and 303 K (Supporting Figure S9)]

as described in chapter "***HuBChE Inhibition Kinetics Studies***" of the "**Experimental Section**". The enzyme concentration was 0.84 nM and the concentration of BTCI was 56 μM. The concentration of compound **(+)-1** were 5 nM and 10 nM and the concentration of **(+)-3** were 1 nM and 2 nM. By progress curve analysis similar to the analysis described in chapter "**Chiral HPLC Resolution and Kinetic Studies of Compound 3**" of the "**Results and Discusion**" section and in chapter "***HuBChE Inhibition Kinetics Studies***" of the "**Experimental Section**", the association and dissociation rate constants at each temperature were determined. Subsequently, Arrhenius plots were constructed (Supporting Figure S10) and the activation enthalpies ($\Delta H^{\ddagger}$) and entropies calculated ($\Delta S^{\ddagger}$).

For the second order association rate constants, as in Equations (2) and (3):

$$\Delta H^{\ddagger} = -(\text{slope} \times 8.314 + (8.314 \times 293)) \quad (2),$$

$$\Delta S^{\ddagger} = \ln(\exp(\text{intercept}) \times 6.626e^{-34}/293/1.38e^{-23}/\exp(1)) \times 8.314 \quad (3),$$

where $\Delta H^{\ddagger}$ is the activation enthalpy, $\Delta S^{\ddagger}$ is the activation entropy and the slope and intercept are of the Arrhenius plot (Supporting Figure S10).

For the first order dissociation rate constants, as in Equations (4) and (5):

$$\Delta H^{\ddagger} = -(\text{slope} \times 8.314) \quad (4),$$

$$\Delta S^{\ddagger} = \ln(\exp(\text{intercept}) \times 6.626e^{-34}/293/1.38e^{-23}) \times 8.314 \quad (5),$$

where $\Delta H^{\ddagger}$ is the activation enthalpy, $\Delta S^{\ddagger}$ is the activation entropy and the slope and intercept are of the Arrhenius plot (Supporting Figure S10).

Activation Gibbs free energies ($\Delta G^{\ddagger}$) were obtained by basic relation, as in Equation (6):

$$\Delta G^{\ddagger} = \Delta H^{\ddagger} - T\Delta S^{\ddagger} \quad (6),$$

where $\Delta G^{\ddagger}$ is the activation Gibbs free energy, $\Delta H^{\ddagger}$ is the activation enthalpy, T is the temperature and $\Delta S^{\ddagger}$ is the activation entropy.

The change of standard Gibss free energy (ΔG^{0}) was calculated by subtracting association activation enthaplies/entropies from dissociation activation enthaplies/entropies. All calculated values are given in Supporting Figure S10 and Figure 7.

The obtained value was checked by converting each inhibition constant ($K_i = k_{off}/k_{on}$) to the corresponding standard Gibbs free energy, as in Equation (7):

$$K_i = \exp(-\Delta G^{0}/RT) \quad (7),$$

where K_i is the inhibition constant, ΔG^{0} is the Gibss free energy, R is the gas constant and T is the temperature.

Computational Analysis of Binding

Computational analysis of binding protocol is described in Supporting Information.

Experiments in Rat Brain Slices

Histochemical Determination of BChE Inhibition

Rats were sacrificed by decapitation under CO_2 anesthesia. The brain of each rat was rapidly removed and immediately frozen on powdered dry-ice, wrapped in Parafilm to prevent desiccation, and stored at −80 °C. Before sectioning the brains, they were left to equilibrate with the temperature of the cryostat chamber, which was adjusted to −20 °C. The brains were cut into sections of 20-μm thickness in a coronal plane using a microtome (SM2000R; Leica) with a freezing stage (Physitemp) and a controller (BFS-30TC). The cytoarchitectonic parcellation of the brain areas was guided by the Atlas of the Adult Rat Brain, by Paxinos and Watson.[78] The section containing the laterodorsal thalamic nucleus was thaw-mounted onto an RNAse-free glass slide coated with a 0.01% solution of (poly)*L*-lysine in dimethylpyrocarbonate, fixed for 5 min in 4% paraformaldehyde, and rinsed (3 × 3 min) in phosphate-buffered saline (PBS) with potassium.

The modified method of Koelle and Friedenwald was used to obtain the histochemical reaction product at the sites of BChE enzyme activity, as described previously.[29] Briefly, the thaw-mounted brain slice sections that included the laterodorsal thalamic nucleus were covered with 30 μL 'Koelle' solution (pH 5.0) containing 3.1 mM copper (II) sulfate, 10 mM glycine, and 50 mM sodium acetate, and with 4 mM butyrylthiocholine iodide as substrate for the BChE. Then, 10 mM 1,5-bis(4-allyldimethylammoniumphenyl)pentan-3-one dibromide was added to the corresponding solutions to completely block AChE. The rat brain slices covered with Koelle solution were incubated for 2 h at 37 °C in a humidity chamber, to prevent evaporation and desiccation of the slices. Following the enzymatic incubation, the sections were rinsed (3 × 3 min) in PBS with potassium (pH 7.4), and placed for 1 min in a developer of 1% sodium sulfide

in distilled water (pH adjusted to 7.5 with glacial acetic acid). Next, the sections were rinsed (3 × 3 min) in distilled water, and the reaction product was intensified for 30 s in 1% silver nitrate solution in distilled water. The staining reaction was terminated by rinses in distilled water (2 × 3 min) and a final rinse in PBS with potassium (3 min). Finally, the sections were dehydrated through a graded ethanol series (50%, 70%, 95%, 100%; 3 min each), cleared with xylene (3 min), and covered with a cover-slip with DPX Mountant for histology.

For the histochemical determination of BChE inhibition, racemic compound **3** was used in the form of its salt. Increasing concentrations of the investigated compound was added to the Koelle solution, to the desired final concentrations (1–300 μM).

Analysis of Butyrycholinesterase-Stained Structures

Stained sections were subjected to extensive microscopy examination using a camera (CoolSNAP; Photometrics, Tuscon, Arizona, USA) and a Northern Light box (Model B90; Imaging Research, St. Cathrines, Ontario, Canada). The investigated brain section was digitalized to produce a high resolution (256 level) grayscale image. A semi-quantitative measure of BChE enzyme activity as the relative optical density score of the staining intensity was determined using the MCID Elite 6.0 software (Imaging Research, St. Catherines, Ontario, Canada).

Cell-Based Assays

Cell Culture and Treatments

The human neuroblastoma SH-SY5Y cell line was purchased from American Type Culture Collection (CRL-2266; Manassas, VA, USA). The cells were cultured in Dulbecco's modified Eagle's medium (Sigma-Aldrich, St. Louis, MO, USA) supplemented with 10% fetal bovine serum (HyClone, Logan, UT, USA), 2 mM *L*-glutamine, 50 U/mL penicillin and 50 μg/mL

streptomycin (all from Sigma), in a humidified atmosphere of 95% air and 5% CO_2 at 37 °C, and grown to 80% confluence. The human hepatocellular HepG2 cell line (ATCC HB-8065, LGC Standards, UK) was cultured in RPMI 1640 medium (Sigma-Aldrich) supplemented with 10% fetal bovine serum (Gibco, Grand Island, NY, USA), 2 mM *L*-glutamine, 100 U/mL penicillin and 100 µg/mL streptomycin (all from Sigma-Aldrich), in a humidified atmosphere of 95% air and 5% CO_2 at 37 °C. Prior to cell treatment, the complete medium was replaced with reduced-serum medium (i.e., with 2% fetal bovine serum). Compound **3** was prepared as a stock solution of 10 mM in DMSO.

Metabolic Activity Assay

The metabolic activities of SH-SY5Y and HepG2 cells were determined using the MTS assay (3-(4,5-dimethylthiazol-2-yl)-5-(3-carboxymethoxyphenyl)-2-(4-sulfophenyl)-2*H*-tetrazolium, inner salt) for the responses to compound **3**. SH-SY5Y cells (2×10^4 cells/well) and HepG2 cells (1×10^4 cells/well) were treated with the appropriate concentrations of the compounds of interest or the corresponding vehicle (control cells) in triplicate in 96-well plates. The metabolic activities were determined after 48 h (SH-SY5Y) or 24 h (HepG2), using the CellTiter 96 Aqueous One Solution Cell Proliferation Assay (Promega, Madison, WI, USA), according to the manufacturer instructions. Absorbance was measured with an automatic microplate reader (Tecan Safire^2, Switzerland) at a wavelength of 492 nm. The data are presented as percentages of the control (DMSO).

***In Vitro* Pharmacokinetics**

Plasma protein binding, stability in human plasma, hepatic metabolic stability, and metabilite identification assays were performed by Eurofins Panlab (St. Charles, MO, USA), in study no.

100028035. In each experiment, the respective reference compounds were tested concurrently with test compound **3**, and the data were compared with historical values determined at Eurofins. The experiment was accepted in accordance with Eurofins validation Standard Operating Procedure.

In Vitro Permeability Assay with Caco-2 Cells

Caco-2 cells were obtained from American Tissue Culture Collection (ATCC HTB.37; lot number 61777387) and were used in the experiments within 1 year. They were grown on Transwell culture inserts with a polycarbonate membrane (diameter, 12 mm; pore size, 0.4 μm). Seeding was at 50,000 cells/filter membrane, and the medium was changed every 2 days. On day 18, the transepithelial electrical resistance was measured for each filter with the Caco-2 cell monolayers. If the transepithelial electrical resistance was in the range of 450 cm^{-2} to 750 cm^{-2}, the Caco-2 cell monolayers were used for the subsequent testing of the permeability on day 21. ABCB1 activity was confirmed with rhodamine123 (Sigma Aldrich, Germany), a selective substrate of ABCB1, which had an efflux ratio of 7.3 (basolateral-to-apical apparent permeability coefficient, 7.7×10^{-6} cm/s; apical-to-basolateral apparent permeability coefficient, 1.1×10^{-6} cm/s). After inhibition with the selective ABCB1 inhibitor PSC833 (Tocris Bioscience, UK), the efflux ratio was reduced to 2.5 (basolateral-to-apical apparent permeability coefficient, 2.5×10^{-6} cm/s; apical-to-basolateral apparent permeability coefficient, 1.0×10^{-6} cm/s). Fluorescence measurements with excitation at 485 nm and emission at 520 nm were used to quantify the rhodamine123 in the samples taken, as described later for compound **3**. The samples were acidified by dilution with the same volume of 0.01 M HCl before the fluorescence measurements.

Ringer buffer with 10 mM D-glucose or 10 mM mannitol was used as the incubation medium, for the apical and basolateral sides of the tissue, respectively. The tissue was kept at 37

°C in a carbogen atmosphere (95% O_2, 5% CO_2) during the experiments. The experiments started with the addition of the stock solution of compound **3**, with fluorescein in the donor compartment to provide the final 100 μM donor concentration of compound **3** and 20 μM fluorescein. The stock solutions were added either to the apical or the basolateral compartment, to obtain bidirectional permeability measurements. Six samples were withdrawn at 20 min intervals, as 150 μL was taken from the 1500 μL basolateral acceptor compartment, and 50 μL from the 500 μL apical acceptor compartment. These volumes were immediately replaced by the appropriate fresh incubation saline. The concentrations of compound **3** in the samples were determined by HPLC-UV immediately after the experiments. The analysis was performed using an Agilent 1100 system (i.e., with a degasser, binary pump, well-plate sampler, column thermostate, diode-array detector) using a Zorbax Eclipse XDB-C18 column (4.6 × 75mm, 3.5 μm) at 55 °C, and a mobile phase of 79% diluted phosphoric acid at pH 2.5 and 21% acetonitrile, at a flow rate of 2.0 mL/min. The injection volume was 40 μL. The detection wavelength was 224 nm, and the retention time was 1.03 min. All of the apparent permeability coefficients were calculated as described previously.[79]

Plasma Protein Binding

Equilibrium dialysis was used to separate the fraction of compound **3** bound to human plasma proteins. The assay was performed in a 96-well format in a dialysis block constructed from Teflon, to minimize nonspecific binding.[80] Human plasma was used as the default protein-containing matrix. Briefly, the protein matrix was spiked with compound **3** at 10 μM (n = 2), and a final DMSO concentration of 1%. Acebutolol, quinidine, and warfarin were tested in each assay as reference compounds, which provided protein binding that was low, medium, and high for the human plasma proteins, respectively. The dialysate compartment was loaded with PBS, pH 7.4,

and the sample side was loaded with an equal volume of the spiked protein matrix. The dialysis plate was then sealed and incubated at 37 °C for 4 h. A control sample (n = 2) was prepared from the spiked protein matrix in the same manner as the assay sample (without dialysis). The control sample served as the basis for determination of the recovery. After the incubation, samples were taken from each compartment, diluted with PBS, followed by addition of acetonitrile, and centrifugation. The supernatants were then used for HPLC-tandem mass spectrometry (MS/MS) analysis using selected reaction monitoring. The HPLC conditions included a binary LC pump with an autosampler, a C18 column (2 × 20 mm), and gradient elution. The peak areas of compound **3** in the buffer and test samples were used to calculate the percent binding and recovery, according to Equations (8) and (9):

$$\text{Protein binding (\%)} = (\text{Area}_p - \text{Area}_b) / \text{Area}_p \times 100 \quad (8),$$

$$\text{Recovery (\%)} = (\text{Area}_p - \text{Area}_b) / \text{Area}_c \times 100 \quad (9),$$

where Area_p is the peak area of the analyte in the protein matrix, Area_b is the peak area of the analyte in the assay buffer, and Area_c is the peak area of the analyte in the control sample.

The recovery determination served as an indicator of the reliability of the calculated protein binding. Low recovery would indicate that the test compound is lost during the course of the assay, which would most likely be due to nonspecific binding or degradation.

Stability in Human Plasma

The stability of compound **3** in human plasma was determined in a 96-well plate format.[81] Human plasma was pre-warmed to 37 °C in a water bath for 5 min, followed by addition of compound **3** at 1 μM, in 0.5% DMSO. Propoxycaine and propantheline were tested at the same time as reference compounds in each assay. The incubation was performed at 37 °C in a water bath over 2 h. An aliquot of the incubation mixture was transferred to acetonitrile at 0, 0.5, 1.0, 1.5 and 2.0 h. These samples were mixed and centrifuged, and their supernatants were used for the HPLC-MS/MS analysis, with selected reaction monitoring. The peak areas were recorded for each analyte. The HPLC conditions included a binary LC pump with autosampler, a C18 column (2 × 20 mm), and gradient elution. The area of the precursor compound that remained after each time point relative to the amount remaining at time zero was calculated as a percentage. Subsequently, the half-life ($t_{1/2}$) was estimated from the slope of the initial linear section of the logarithmic curve of the compound remaining (%) *versus* time, assuming first-order kinetics. The positive control experiment showed results as expected for propantheline ($t_{1/2}$ = 18 min) and propaxycaine ($t_{1/2}$ = 3 min).

Hepatic Metabolic Stability

The metabolic stability of compound **3** was determined in a 96-well plate format.[82] This used human cryopreserved hepatocytes; aand was expressed as the intrinsic clearance (Cl_{int}). The cryopreserved hepatocytes were from a mixed gender pool of 10 or more human subjects, and they were thawed, washed, and resuspended in Krebs-Heinseleit buffer (pH 7.3). The reaction was initiated by adding compound **3** at 1 μM (final DMSO concentration, 0.01%) into the cell suspension (final cell density, 0.7×10^6 viable cells/mL), and incubated for 0, 0.5, 1.0, 1.5 and 2.0 h, at 37 °C and 5% CO_2. The reaction was stopped by adding acetonitrile into the incubation mixture. The samples were then mixed, transferred completely to another 96-well plate, and

centrifuged. The supernatants were used for HPLC-MS/MS analysis. As reference substances, four compounds were tested in each assay. Propranolol is relatively stable, whereas flurazepam, naloxone, and 7-hydroxy-4-trifluoromethylcoumarin are readily metabolized by human hepatocytes. In the HPLC-MS/MS analysis, the peak areas corresponding to the test compounds were recorded. Metabolic stabilities were expressed as the percentages of the parent compounds remaining, and were calculated by comparing the peak area of the compound at the time point relative to time 0. The half-life ($t_{1/2}$) was estimated from the slope of the initial linear range of the logarithmic curve of the compound remaining (%) *versus* time, assuming first-order kinetics. The apparent intrinsic clearance (Cl_{int}, in μL/min/million cells) was calculated from $t_{1/2}$ according to Equation (10):

$$Cl_{int} = 0.693 / (t_{1/2} \times 10^6 \text{ cells}/\mu L) \quad (10).$$

Metabolite Identification

Principal phase I (oxidative) and phase II (conjugative) metabolites have been detected and characterized following previously described preocedures.[82] Briefly, compound **3** (10 μL) was incubated at 37 °C with cryopreserved human hepatocytes (0.7×10^6 cells/mL) for 2 h. Samples were taken at time 0 and at the end of the incubation. A control sample (no compound **3** added) was also prepared and incubated for the same period of time. After the reaction was stopped by addition of acetonitrile, the supernatants underwent HPLC-MS analysis. Separation of the analytes was achieved using an Acquity HSS T3 column (100 × 2.1 mm, 1.8 μm; Waters). These samples (5 μL) were injected onto the system and eluted at a flow rate of 0.5 mL/min using a linear gradient of mobile phase A (0.1% formic acid in water) and mobile phase B (0.1% formic acid in MeCN). The gradient for mobile phase B was: 0–1.0 min, 5%; 1.0–7.0 min, 5%–80%;

7.0–7.5 min, 80%; 7.5–8.0 min, 80%–5%; 8.0–10.0 min, 5%. The HPLC was interfaced to a Waters Xevo G2 QTOF system using electrospray ionization (source temperature, 150 °C; desolvation temperature, 400 °C; desolvation gas, 400 L/h; capillary, 0.75 kV; sampling cone voltage, 50 V; extraction cone voltage, 2.7 V). A full-scan analysis in positive mode was performed over a mass-to-charge range suitable to cover the expected phase I and phase II metabolic products of the test compounds (200-800 Da). An MS^E acquisition method was used, which uses a high and low collision energy function, such that the precursor (MS) and product ion (MS/MS) information on all of the analytes in the sample is collected in a single analysis. Full-scan total ion chromatograms were obtained from time 0 and 2 h, and also for a blank matrix sample, and were compared using the MetaboLynx software package of the MS system. The sample data files were thus processed in an automated fashion to look for expected and unexpected metabolic products, and unique peaks in the incubation samples were directly compared to the control sample. Retention times and the respective MS and MS/MS spectra of the species detected in the samples and not in the time-zero or blank samples were identified and recorded.

In Vivo Blood Plasma–Brain Distribution

Animals

The blood plasma–brain distribution of compound **3** was measured in 3-month-old female Wistar Han rats (body weight, 220 g ±10%). The rats were handled according to the European Community Council Directive of 23 November 1986 (86/609/EEC), and the National Veterinary Institute Guide for the Care and Use of Laboratory animals. The experimental design was evaluated by the National Ethical Committee for Animal Experimentation, and approved by the Administration of the Republic of Slovenia for food safety, veterinary and plant protection. All

efforts were made to minimize the number of rats used and their suffering. The animals were monitored for any behavioral signs of discomfort from application of the test compounds until euthanasia.

Chemicals used in the blood plasma–brain distribution assay

Here, 10 mg/mL compound **3** was dissolved in 1% Tween 80 in isotonic sodium chloride, and sterilized by filtration. The isotonic 1% Tween 80 alone was used as the negative control, and 2 mg/mL donepezil in the same solution was used as the positive control.

In vivo blood plasma–brain distribution assay, sample collection and work up

Four rats were given compound **3** and three rats were used for each of the positive and negative controls. Compound **3** and donepezil were injected intraperitoneally at 10 mg/kg and 2 mg/kg, respectively. The rats were euthanized by CO_2 inhalation 1 h after administration of compound **3**. Immediately, 2 mL blood was collected in tubes (Vacutainer) with 10.8 mg K_2EDTA, and the brain tissue was isolated. Blood plasma was obtained after centrifugation of the blood at 3,500 rpm for 10 min. The blood plasma and brain tissue were stored at –20 °C until further sample preparation.

Four aliquots of approximately 150 mg of each brain tissue sample were weighed and homogenized in 2-mL microcentrifuge tubes (Eppendorf, Germany) with 25 µL internal standard solution (450 µg/L haloperidol in 80% MeOH with 0.1% acetic acid), 300 µL PBS, and 125 µL methanol, in a blender (Bullet Blender; Next Advance, NY, USA) for 3 min at speed setting ‘8’ with 0.5-mm diameter glass beads. The homogenate was centrifuged at 10,000 rpm for 7 min, and the supernatant was removed. The sample was mixed again in the blender for 1 min at speed setting ‘5’, and a second supernatant was collected after centrifugation as before. These

supernatants were then combined and 900 µL 2% H_3PO_4 was added prior to solid phase extraction.

Blood plasma aliquots (150 µL) in 2-mL microcentrifuge tubes (Eppendorf) were mixed with 25 µL internal standard solution (450 µg/L haloperidol in 80% MeOH with 0.1% acetic acid), 300 µL PBS and 125 µL MeOH. The samples were mixed in the blender for 1 min at minimum speed, and bath sonicated for 5 min. Then 900 µL 2% H_3PO_4 was added in two aliquots during the quantitative sample transfer to the solid phase extraction column.

For the preparation of all of the samples for LC-MS/MS quantification, Bond Elut Plexa PCX (30 mg, 3 mL) solid phase extraction columns were used. Before the samples were slowly loaded, these columns were conditioned with 2 mL methanol and equilibrated with 2 mL water. Then 2 mL 2% formic acid, followed by 2 mL MeOH/MeCN (1:1, v/v) were used for column washing. The samples were eluted with 1 mL 25% ammonia in water/MeOH/MeCN (1:2:2, v/v), and dried for 20 min in a concentration evaporator (Turbovap) at 60 °C. The dried samples were stored at –20 °C until analysis. The samples were reconstituted in 200 µL 0.1% acetic acid in 80% MeOH using 2 × 2 min mixing in the blender at minimum speed, separated by a 10 min interval.

For calculation of the brain-to-plasma ratio of compound **3**, its concentration in the brain (µg/kg) and its concentration in the blood plasma (µg/L) were determined, and the specific density of wet rat brain of 1.05 g/mL was used.[83]

LC-MS/MS Analysis

For quantification, the reconstituted samples were analyzed by UHPLC-MS/MS, which included a liquid cromatograph (Agilent 1290) and a triple quadrupole mass spectrometer (Agilent 6460) connected through the JetStream electrospray ionization ion source interface (Agilent

Techologies, Santa Clara, USA). Chromatographic separation was performed on a C18 column (50 × 2.1 mm; 2.6 μm; Kinetex), with a C18 cartridge guard column (4 × 2.0 mm; Phenomenex, Torrance, USA) and kept at 50 °C. The injection volume was 0.50 μL. After each injection, the injection needle was washed for 6 s with 80% MeOH. Mobile phase A was 0.05% formic acid in water, and mobile phase B was MeCN. The flow rate was 0.65 mL/min with the following gradient (as %B): 0–0.25 min, 10%–15%; 0.25–0.5 min, 15%–28%; 0.5–1.0 min, 28%–45%; 1.0–1.25 min, 45%–55%; 1.25–2.0 min, 55%–65%; 2.0–2.1 min, 65%–10%. The total run time including re-equlibration was 2.8 min. The ion source parameters were set as follows: drying gas temperature, 275 °C; drying gas flow rate, 5 L/min; nebulizer, 45 PSI (3.1×10^5 Pa); sheath gas temperature, 320 °C; sheath gas flow, 11 L/min; capillary entrance voltage, 4000 V; nozzle voltage, 1000 V; and delta EMV, 200 V. MRM transitions and fragmentation parameters for analytes quantified by UHPLC-MS/MS are given in Supporting Table S10.

The instrument control, and data acquisition and quantification were performed using the MassHunter Workstation software B.06.00 (Agilent Technologies, Torrance, USA). MRM chromatograms for the signal-to-noise ratios are shown in Supporting Figure S14.

LC-MS/MS Method Validation

The LC-MS/MS method was tested for accuracy, precision, linear range, limit of quantification, recovery, matrix effects, and stability, according to the US Food and Drug Administration Guidance for Bioanalytical Method Validation.[84]

The linear range was determined as the range of the calibration samples with acceptable accuracy (±15% bias) and precision (15% relative standard deviation (RSD)). The calibration samples were prepared by spiking known amounts of standards dissolved in 80% methanol into blank blood plasma and blank brain tissue prior to the homogenization and extraction procedures.

The added volume of the stock solution to 150 μL plasma or 150 mg brain tissue was from 10 μL to 150 μL at each of 10 levels, and the organic solvent addition was kept constant for all of the samples. The concentration ranges for donepezil and compound **3** in plasma were 2 μg/L to 300 μg/L and 0.5 μg/L to 75 μg/L, respectively. The concentration range of both donepezil and compound **3** in brain tissue was 1 μg/kg to 150 μg/kg. The measured responses across the whole range were linear, and showed good correlation, with determination coefficients of 0.99 or greater.

The limit of quantification was set at the lowest calibration level that showed acceptable accuracy (bias < ±20%) and precision (<20% RSD), with the peak area at least 5-fold greater than the response of the processed blank sample at the same retention time, and with a signal-to-noise ratio of at least 30:1 (root mean square). The limits of quantification for donepezil were 2.5 μg/L and 2.0 μg/kg in plasma and brain tissue, respectively. The limits of quantification for compound **3** were 1.25 μg/L and 5 μg/kg in plasma and brain tissue, respectively.

Quality control samples were prepared the same way as for the calibration, except with different weighings and at only three different levels: Low, medium and high (Supporting Table S11).

Accuracy was determined by comparing the measured concentrations of the quality control samples to their true values, and expressed as bias (%). Method repeatability was determined by calculating the RSD from the separately prepared and analyzed quality control samples. These data are presented in Supporting Table S12.

The extraction recovery, absolute matrix effects, and relative matrix effects were determined as reported previously[85] at two quality control levels: low and high. Briefly, the recovery was calculated as the ratio between the peak area response from the quality control

samples spiked before the extraction (A), and the peak areas from the samples spiked at the same levels after the extraction of the blank samples (B), as in Equation (11):

$$\text{Extraction recovery (\%)} = A/B \times 100 \quad (11).$$

The absolute matrix effect was calculated as the ratio between the peak area response from the quality control samples spiked before extraction (A), and the peak area response from the samples spiked with pure reconstitution solvent at the same levels (C), as in Equation (12):

$$\text{Absolute matrix effect (\%)} = A/C \times 100 \quad (12).$$

The relative matrix effect was calculated as the RSD from the quality control samples spiked in blank matrices obtained from four different untreated donors. The recovery and matrix effect data are presented in Supporting Table S13.

The stability experiments covered the following conditions: stock solution stability (refrigerator at 4 °C, 7 days), freeze/ thaw stability (4 cycles), short-term stability (4 h at 25 °C), long term stability (14 days at –20 °C), and autosampler stability (reconstituted samples, 48 h at 4 °C). The data showed no detectable mean analyte peak area deterioration compared to the time zero measurements (deviation <15% RSD). Indeed, in some samples, the signal responses were even higher at later time points, most probably due to solvent evaporation from closed vessels.

In Vivo Activity Assays

Animals

C57BL/6J mice from the Animal Breeding Farm in Children's Hospital of the Jagiellonian University were used in the Morris water maze (MWM) task. Six-week-old male Albino Swiss (CD-1) mice from the Animal Breeding Farm at the Faculty of Pharmacy, Jagiellonian University (18-24 g) were used in the locomotor activity and rotarod tests. Before the experiments, the animals were housed in groups of 10 mice per cage at a room temperature of 22 ±2 ^{o}C, under a light/ dark (12:12 h) cycle. The animals had free access to food and water before the tests. The ambient temperature of the room and relative humidity (50%) were kept consistent throughout all of the tests. For the behavioral experiments, the mice were selected at random. Each experimental group consisted of 8 to 10 mice/dose. The experiments were performed between 08:00 hours and 14:00 hours. Immediately after the *in vivo* assays the mice were euthanized by cervical dislocation. The procedures for maintenance and treatment of laboratory animals were approved by the Local Ethics Committee of the Jagiellonian University in Krakow.

Chemicals used in the in vivo assays

In the *in vivo* experiments, compound **3** was tested at a dose 30 mg/kg intraperitoneally in the MWM task. It was suspended in 1% Tween 80 (Polskie Odczynniki Chemiczne, Poland) and was administered 60 min before the behavioral tests. Donepezil hydrochloride (Sigma Aldrich, Poland) was dissolved in distilled water. In the MWM task it was tested at 10 mg/kg intraperitoneally. Control mice were given the appropriate amount of vehicle (1% Tween 80).

(–)-Scopolamine hydrobromide (Sigma Aldrich; Poland) was used to induce memory impairment in the mice. It was dissolved in distilled water and was administered intraperitoneally at 1 mg/kg, 30 min before the acquisition phase of the MWM tasks.

Behavioral Testing Paradigms

Morris Water Maze Task

The Morris water maze is a circular, plastic, gray-painted pool (diameter, 1.20 m; height 0.60 m) that is filled with water (up to about 48 cm below the edge, to prevent animals from jumping out) maintained at 23 ±1 °C. The pool is divided into four equal quadrants (compass locations: NE, NW, SE, SW) using a computerized video tracking system (SMART, version 3.0; Panlab, Spain). An escape platform made of transparent Plexiglas (diameter, 11 cm; height, 47 cm) is positioned at a fixed location (the center of the NW quadrant; i.e., the target quadrant), with this invisible to the swimming animal. It is immersed 1 cm under the surface of the water. During the experiments the maze is lit with a light intensity of 45 lx.

In the spatial acquisition trial (6 consecutive days), the mice were assigned to training sessions (four training sessions per day; sessions held 4 h apart) in which the mice were trained to escape from the water by reaching the hidden platform, the location of which can be identified using distal extra-maze cues attached to the room walls (i.e., A4-sized sheets of black laminated paper with colored geometric symbols), which constitute the navigation points.[86,87] These visual cues have different colors and dimensions and were kept constant during the whole experiment.[87] The whole experiment was conducted by an experimenter who always remained stationary in a constant location, as an additional distal cue for the swimming mice. For each trial, the mouse was placed in the water starting from a different randomly chosen quadrant that did not contain the platform, whereas the platform was always positioned in the same place. If an animal did not find the hidden platform within 60 s, it was gently placed on the platform for 15 s. The time taken to reach the hidden platform (i.e., escape latency time), the distance traveled to reach the hidden platform, the distance (%) in the target (NW) zone, and mean speed were recorded.

On day 7 (24 h after the last training session), the platform was removed from the pool and a probe trial was performed (drug-off trial). Each mouse was allowed to swim for 60 s. If a

mouse did not find the previous platform position within 60 s, it was given a latency score of 60 s.[86,88] The latency time to the first crossing of the former platform location (i.e., the target zone), the number of crossings of the target zone, the time (%) spent in the target NW quadrant, the total distance, the distance (%) spent in the NW quadrant, the entries into the NW quadrant, and the mean speed were measured and compared across the experimental groups.

Locomotor activity assay

Before the locomotor activity test, the mice were habituated to activity cages for 30 min. The test was performed using activity cages (40 cm × 40 cm × 30 cm; supplied with infrared beam emitters; Activity Cage 7441; Ugo Basile, Italy) connected to a counter for the recording of the light-beam interruptions. Sixty min before the experiment, the mice were pretreated with compound **3** or the vehicle intraperitoneally, then they were individually placed in the activity cages in a sound-attenuated room. The number of light-beam crossings was counted for compound **3**-treated and vehicle-treated mice over the following 30 min of the test.[89]

Rotarod test

Before the rotarod test, the animals were trained daily for 3 consecutive days on the rotarod apparatus (Rotarod apparatus, May Commat RR0711, Turkey; rod diameter, 2 cm) that was rotating at a fixed speed of 18 rotations per minute (rpm). In each training session, the mice were put on the rotating rod for 3 min with an unlimited number of trials. The actual experiment was performed 24 h after the last training session. Sixty min after the administration of compound **3** (30 mg/kg) or vehicle intraperitoneally, the mice were tested on the rod revolving at 6, 18 or 24 rpm. Motor impairment was defined as the inability to remain on the rotarod appatatus for 1 min, and is expressed as the mean time spent on the rotarod.[89]

Data analysis

Data analysis of the *in vivo* results was performed using GraphPad Prism software (version 5; CA, USA). The numerical results from the tests are expressed as means ±standard error of the mean (SEM). For the statistical analysis, one-way analysis of variance (ANOVA) followed by Dunnett's *post-hoc* comparisons, or repeated measures ANOVA followed by Bonferroni multiple comparisons, were used. $P < 0.05$ was considered significant.

AUTHOR INFORMATION

Corresponding Author

* Tel: +386-1-4769585. Fax: +386-1-4258031. E-mail: Stanislav.gobec@ffa.uni-lj.si.

Author contributions

The manuscript was written through contributions of all of the authors. All of the authors have indicated their approval of the final version of the manuscript.

Notes

The authors declare no competing financial interests.

ACKNOWLEDGMENT

The authors acknowledge the financial support from the Slovenian Research Agency (research core funding No. P1-0208 and P4-0127, project L1-8157, and bilateral project ARRS-CEA to S.G.), the Agence Nationale de la Recherche (ANR) (project Multi-Click, grant number ANR-12-

BS07-0008-01 to J.-P.C.), and the France Alzheimer Foundation (grant FA-AAP-2013-65-101349 to J.-P.C.). This study was also supported by the France-Alzheimer Foundation, the Agence Nationale de la Recherche (ANR), and Institut Francais. We thank Domen Kutoša, Urša Jarc, Julija Lipušček, Aljoša Jelenko and Matevž Černigoj for their contributions. We thank Dr. Dušan Žigon (Jožef Stefan Institute, Ljubljana, Slovenia) for performing the mass spectrometry measurements, and Dr. Chris Berrie for critical reading of the manuscript.

ABBREVIATIONS

Aβ, amyloid-β; AChE, acetylcholinesterase; AD,Alzheimer's disease; BChE, butyrycholinesterase; BTCI, butyrylthiocholine iodide; ChEs, cholinesterases; CHO, chinese hamster ovary; DMF, dimethylformamide; DMSO, dimethyl sulfoxide; DTNB, 5,5′-dithiobis (2-nitrobenzoic acid); huBChE, human butyrycholinesterase; mAChE, murine acetylcholinesterase; MTS, 3-(4,5-dimethylthiazol-2-yl)-5-(3-carboxymethoxyphenyl)-2-(4-sulfophenyl)-2*H*-tetrazolium, inner salt; MWM, Morris water maze; NE, north east; NW, north west; P_{app}, permeability values. PBS, phosphate-buffered saline; PDB, protein data bank; RSD, relative standard deviation; SE, south east; SEM, standard error of the mean; SW, south west; TBTU, 2-(1*H*-benzotriazole-1-yl)-1,1,3,3-tetramethylaminium tetrafluoroborate; TFA, 2,2,2-trifluoroacetic acid

ASSOCIATED CONTENT

Supporting Information

Supportin Information is available.

Supporting Figures S1-S14, Supporting Tables S1-S13, Supporting Discussion (Synthesis, Structure-Activity Relationships), Synthesis and Characterization of Compounds, Computational Analysis of Binding Protocol and Molecular Formula Strings.

REFERENCES

1. Price, M.; Comas-Herrera, A.; Knapp, M.; Guerchet, M.; Karagiannidou, M. *The World Alzheimer Report 2016*; Alzheimer's Disease International (ADI): London, 2016; pp 1-131.
2. Brookmeyer, R.; Johnson, E.; Ziegler-Graham, K.; Arrighi, H. M. Forecasting the Global Burden of Alzheimer's Disease. *Alzheimer's Dementia* **2007**, *3*, 186-191.
3. Morris, M.; Knudsen, G. M.; Maeda, S.; Trinidad, J. C.; Ioanoviciu, A.; Burlingame, A. L.; Mucke, L. Tau Post-Translational Modifications in Wild-Type and Human Amyloid Precursor Protein Transgenic Mice. *Nat. Neurosci.* **2015**, *18*, 1183-1189.
4. Glabe, C. C. Amyloid Accumulation and Pathogensis of Alzheimer's Disease: Significance of Monomeric, Oligomeric and Fibrillar Aβ. In *Alzheimer's Disease*; Harris, J. R., Fahrenholz, F., Eds.; Subcellular Biochemistry; Springer US: New York, 2005; pp 167–177.
5. Sinha, S.; Lieberburg, I. Cellular Mechanisms of β-Amyloid Production and Secretion. *Proc. Natl. Acad. Sci. U. S. A.* **1999**, *96*, 11049-11053.
6. Gella, A.; Durany, N. Oxidative Stress in Alzheimer Disease. *Cell Adhes. Migr.* **2009**, *3*, 88-93.
7. Donev, R.; Kolev, M.; Millet, B.; Thome, J. Neuronal Death in Alzheimer's Disease and Therapeutic Opportunities. *J. Cell. Mol. Med.* **2009**, *13*, 4329-4348.
8. Bartus, R. T.; Dean, R. L.; Beer, B.; Lippa, A. S. The Cholinergic Hypothesis of Geriatric Memory Dysfunction. *Science* **1982**, *217*, 408-414.
9. Bartus, R. T. On Neurodegenerative Diseases, Models, and Treatment Strategies: Lessons Learned and Lessons Forgotten a Generation Following the Cholinergic Hypothesis. *Exp. Neurol.* **2000**, *163*, 495-529.

10. Reid, G. A.; Chilukuri, N.; Darvesh, S. Butyrylcholinesterase and the Cholinergic System. *Neuroscience* **2013**, *234*, 53-68.
11. Giacobini, E. Cholinomimetic Replacement of Cholinergic Function in Alzheimer Disease. In *Treatment of Dementias: A New Generation of Progress*, 1st ed; Meyer, E. M., Simpkins, J. W., Yamamoto, J., Crews, F. T., Eds.; Springer: New York, 1992; pp 19-34.
12. Scarpini, E.; Schelterns, P.; Feldman, H. Treatment of Alzheimer's disease: Current Status and New Perspectives. *Lancet Neurol.* **2003**, *2*, 539-547.
13. Sugimoto, H.; Iimura, Y.; Yamanishi, Y.; Yamatsu, K. Synthesis and Structure-Activity Relationships of Acetylcholinesterase Inhibitors: 1-Benzyl-4-[(5,6-Dimethoxy-1-Oxoindan-2-yl)methyl]piperidine Hydrochloride and Related Compounds. *J. Med. Chem.* **1995**, *38*, 4821-4829.
14. Bar-On, P.; Millard, C. B.; Harel, M.; Dvir, H.; Enz, A.; Sussman, J. L.; Silman, I. Kinetic and Structural Studies on the Interaction of Cholinesterases with the Anti-Alzheimer drug Rivastigmine. *Biochemistry* **2002**, 41, 3555–3564.
15. Greenblatt, H. M.; Kryger, G.; Lewis, T.; Silman, I.; Sussman, J. L. Structure of Acetylcholinesterase Complexed with (–)-Galanthamine at 2.3 A Resolution. *FEBS Lett.* **1999**, *463*, 321-326.
16. Tago, H.; Maeda, T.; McGeer, P. L.; Kimura, H. Butyrylcholinesterase-rich Neurons in Rat Brain Demonstrated by a Sensitive Histochemical Method. *J. Comp. Neurol.* **1992**, *325*, 301-312.
17. Darvesh, S.; Grantham, D. L.; Hopkins, D. A. Distribution of Butyrylcholinesterase in the Human Amygdala and Hippocampal Formation. *J. Comp. Neurol.* **1998**, *393*, 374-390.
18. Geula, C.; Nagykery, N. Butyrylcholinesterase Activity in the Rat Forebrain and Upper Brainstem: Postnatal Development and Adult Distribution. *Exp. Neurol.* **2007**, *204*, 640-657.

19. Mesulam, M.; Guillozet, A.; Shaw, P.; Quinn, B. Widely Spread Butyrylcholinesterase can Hydrolyze Acetylcholine in the Normal and Alzheimer Brain. *Neurobiol. Dis.* **2002**, *9*, 88-93.

20. Mesulam, M.-M.; Guillozet, A.; Shaw, P.; Levey, A.; Duysen, E. .; Lockridge, O. Acetylcholinesterase Knockouts Establish Central Cholinergic Pathways and can use Butyrylcholinesterase to Hydrolyze Acetylcholine. *Neuroscience* **2002**, *110*, 627-639.

21. Darvesh, S.; Hopkins, D. A.; Geula, C. Neurobiology of Butyrylcholinesterase. *Nat. Rev. Neurosci.* **2003**, *4*, 131-138.

22. Giacobini, E. *Butyrylcholinesterase: Its Function and Inhibitors*; Taylor & Francis Group: London, 2003.

23. Duysen, E. G.; Li, B.; Darvesh, S.; Lockridge, O. Sensitivity of Butyrylcholinesterase Knockout Mice to (–)-Huperzine A and Donepezil Suggests Humans with Butyrylcholinesterase Deficiency may not Tolerate these Alzheimer's Disease Drugs and Indicates Butyrylcholinesterase Function in Neurotransmission. *Toxicology* **2007**, *233*, 60-69.

24. Perry, E. K.; Perry, R. H.; Blessed, G.; Tomlinson, B. E. Changes in Brain Cholinesterases in Senile Dementia of Alzheimer Type. *Neuropathol. Appl. Neurobiol.* **1978**, *4*, 273-277.

25. Davies, P.; Maloney, A. J. Selective Loss of Central Cholinergic Neurons in Alzheimer 's Disease. *Lancet* **1976**, 2, 1403.

26. Ciro, A.; Park, J.; Burkhard, G.; Yan, N.; Geula, C. Biochemical Differentiation of Cholinesterases from Normal and Alzheimer's Disease Cortex. *Curr. Alzheimer Res.* **2012**, *9*, 138-143.

27. Giacobini, E. Cholinergic Function and Alzheimer's Disease. *Int. J. Geriatr. Psychiatry* **2003**, *18*, S1–S5.

28. Greig, N. H.; Utsuki, T.; Ingram, D. K.; Wang, Y.; Pepeu, G.; Scali, C.; Yu, Q.-S.; Mamczarz, J.; Holloway, H. W.; Giordano, T.; Chen, D.; Furukawa, K.; Sambamurti, K.; Brossi, A.; Lahiri, D. K. Selective Butyrylcholinesterase Inhibition Elevates Brain Acetylcholine, Augments Learning and Lowers Alzheimer β-Amyloid Peptide in Rodent. *Proc. Natl. Acad. Sci. U. S. A.* **2005**, *102*, 17213-17218.

29. Košak, U.; Brus, B.; Knez, D.; Šink, R.; Žakelj, S.; Trontelj, J.; Pišlar, A.; Šlenc, J.; Gobec, M.; Živin, M.; Tratnjek, L.; Perše, M.; Sałat, K.; Podkowa, A.; Filipek, B.; Nachon, F.; Brazzolotto, X.; Więckowska, A.; Malawska, B.; Stojan, J.; Mlinarič Raščan, I.; Kos, J.; Coquelle, N.; Colletier, J. P.; Gobec, S. Development of an In-Vivo Active Reversible Butyrylcholinesterase Inhibitor. *Sci. Rep.* **2016**, *6*, 39495.

30. Furukawa-Hibi, Y.; Alkam, T.; Nitta, A.; Matsuyama, A.; Mizoguchi, H.; Suzuki, K.; Moussaoui, S.; Yu, Q.-S.; Greig, N. H.; Nagai, T.; Yamada, K. Butyrylcholinesterase Inhibitors Ameliorate Cognitive Dysfunction Induced by Amyloid-β Peptide in Mice. *Behav. Brain Res.* **2011**, *225*, 222-229.

31. Hartmann J.; Kiewert, C.; Duysen, E. G.; Lockridge, O.; Greig, N. H.; Klein, J. Excessive Hippocampal Acetylcholine Levels in Acetylcholinesterase-Deficient Mice are Moderated by Butyrylcholinesterase Activity. *J. Neurochem.* **2007**, *100*, 1421-1429.

32. Giacobini, E. Cholinesterase Inhibitors: New roles and Therapeutic Alternatives. *Pharmacol. Res.* **2004**, *50*, 433-440.

33. McGleenon, B. M.; Dynan, K. B.; Passmore, A. P. Acetylcholinesterase Inhibitors in Alzheimer's Disease. *Br. J. Clin. Pharmacol.* **1999**, *48*, 471-480.

34. Ballard, C.; Greig, N.; Guillozet-Bongaarts, A.; Enz, A.; Darvesh, S. Cholinesterases: Roles in the Brain During Health and Disease. *Curr. Alzheimer Res.* **2005**, *2*, 307-318.

35. Brus, B.; Košak, U.; Turk, S.; Pišlar, A.; Coquelle, N.; Kos, J.; Stojan, J.; Colletier, J. P.; Gobec, S. Discovery, Biological Evaluation, and Crystal Structure of a Novel Nanomolar Selective Butyrylcholinesterase Inhibitor. *J. Med. Chem.* **2014**, *57*, 8167-8179.

36. Summers, W. K.; Majovski, L. V.; Marsh, G. M.; Tachiki, K.; Kling, A. Oral Tetrahydroaminoacridine in Long-Term Treatment of Senile Dementia, Alzheimer type. *N. Engl. J. Med.* **1986**, *315*, 1241-1245.

37. Decker, M. Homobivalent Quinazolinimines as Novel Nanomolar Inhibitors of Cholinesterase with Dirigible Selectivity Towards Butyrylcholinesterase. *J. Med. Chem.* **2006**, *49*, 5411-5413.

38. Rizzo, S.; Rivière, C.; Piazzi, L.; Bisi, A.; Gobbi, S.; Bartolini, M.; Andrisano, V.; Morroni, F.; Tarozzi, A.; Monti, J. P.; Rampa, A. Benzofuran-Based Hybrid Compounds for the Inhibition of Cholinesterase Activity, β Amyloid Aggregation, and Aβ Neurotoxicity. *J. Med. Chem.* **2008**, *51*, 2883-2886.

39. Darvesh, S.; Darvesh, K. V.; McDonald, R. S.; Mataija, D.; Walsh, R.; Mothana, S.; Lockridge, O.; Martin, E. Carbamates with Differential Mechanism of Inhibition Toward Acetycholinesterase and Butyrycholinesterase. *J. Med. Chem.* **2008**, *51*, 4200-4212.

40. Carolan, C. G.; Dillon, G. P.; Khan, D.; Ryder, S. A.; Gaynor, J. M.; Reidy, S.; Marquez, J. F.; Jones, M.; Holland, V.; Gilmer, J. F. Isosorbide-2-Benzyl Carbamate-5-Salicylate, a Peripheral Anionic Site Binding Subnanomolar Selective Butyrylcholinesterase Inhibitor. *J. Med. Chem.* **2010**, *53*, 1190-1199.

41. Zha, X.; Lamba, D.; Zhang, L.; Lou, Y.; Xu, C.; Kang, D.; Chen, L.; Xu, Y.; Zhang, L.; De Simone, A.; Samez, S.; Pesaresi, A.; Stojan, J.; Lopez, M. G.; Egea, J.; Andrisano, V.; Bartolini, M. Novel Tacrine-Benzofuran Hybrids as Potent Multitarget-Directed Ligands for

the Treatment of Alzheimer's Disease: Design, Synthesis, Biological Evaluation, and X-Ray Crystallography. *J. Med. Chem.* **2016**, 59, 114-131.

42. Lipinski, C. A.; Lombardo, F.; Dominy, B. W.; Feeney, P. J. Experimental and Computational Approaches to Estimate Solubility and Permeability in Drug Discovery and Development Settings. *Adv. Drug Delivery Rev.* **2001**, *46*, 3-26.
43. Cui, M.; Ono, M.; Kimura, H.; Ueda, M.; Nakamoto, Y.; Togashi, K.; Okamoto, Y.; Ihara, M.; Takahashi, R.; Liu, B.; Saji, H. Novel 18F-Labeled Benzoxazole Derivatives as Potential Positron Emission Tomography Probes for Imaging of Cerebral β-Amyloid Plaques in Alzheimer's Disease. *J. Med. Chem.* **2012**, *55*, 9136-9145.
44. Nicolet, Y.; Lockridge, O.; Masson, P.; Fontecilla-Camps, J. C.; Nachon, F. Crystal Structure of Human Butyrylcholinesterase and of its Complexes with Substrate and Products. *J. Biol. Chem.* **2003**, *278*, 41141-41147.
45. Košak, U.; Brus, B.; Gobec, S. Straightforward Synthesis of Orthogonally Protected Piperidin-3-ylmethanamine and Piperidin-4-ylmethanamine Derivatives. *Tetrahedron Lett.* **2014**, *55*, 2037-2039.
46. Ellman, G. L.; Courtney, K. D.; Andres jr., V.; Featherstone, R. M. A New and Rapid Colorimetric Determination of Acetylcholinesterase Activity. *Biochem. Pharmacol.* **1961**, *7*, 88-95.
47. Kryger, G.; Harel, M.; Giles, K.; Toker, L.; Velan, B.; Lazar, A.; Kronman, C.; Barak, D.; Ariel, N.; Shafferman, A.; Silman, I.; Sussman, J. L. Structures of Recombinant Native and E202Q Mutant Human Acetylcholinesterase Complexed with the Snake-Venom Toxin Fasciculin-II. *Acta Crystallogr., Sect. D: Biol. Crystallogr.* **2000**, *56*, 1385-1394.
48. Copeland, R. A. *Evaluation of Enzyme Inhibitors in Drug Discovery: A Guide for Medicinal Chemists and Pharmacologists*; John Wiley & Sons: Hoboken, 2013; pp 245–285.

49. Bevc, S.; Konc, J.; Stojan, J.; Hodošček, M.; Penca, M.; Praprotnik, M.; Janežič, D. ENZO: A Web Tool for Derivation and Evaluation of Kinetic Models of Enzyme Catalyzed Reactions. *PLoS ONE* **2011**, *6*, e22265.
50. Bolognesi, M. L.; Bartolini, M.; Mancini, F.;, Chiriano, G.; Ceccarini, L.; Rosini, M.; Milelli, A.; Tumiatti, V.; Andrisano, V.; Melchiorre, C. Bis(7)-tacrine Derivatives as Multitarget-Directed Ligands: Focus on Anticholinesterase and Antiamyloid Activities. *ChemMedChem* **2010**, *5*, 1215–1220.
51. Darras, F. H.; Pang, Y. P. On the Use of the Experimentally Determined Enzyme Inhibition Constant as a Measure of Absolute Binding Affinity. *Biochem. Biophys. Res. Commun.* **2017**, *489*, 451–454.
52. Koelle, G. B.; Friedenwald, J. A. A Histochemical Method for Localizing Cholinesterase Activity. *Proc. Soc. Exp. Biol. Med.* **1949**, *70*, 617-622.
53. Darvesh, S.; Grantham, D. L.; Hopkins, D. A. Distribution of Butyrylcholinesterase in the Human Amygdala and Hippocampal Formation. *J. Comp. Neurol.* **1998**, *393*, 374-390.
54. Geula, C.; Nagykery, N. Butyrylcholinesterase Activity in the Rat Forebrain and Upper Brainstem: Postnatal Development and Adult Distribution. *Exp. Neurol.* **2007**, *204*, 640–657.
55. Žakelj, S.; Berginc, K.; Roškar, R.; Kraljič, B.; Kristl, A. Do the Recommended Standards for in Vitro Biopharmaceutic Classification of Drug Permeability Meet the "Passive Transport" Criterion for Biowaivers? *Curr. Drug Metab.* **2013**, *14*, 21-27.
56. Di, L.; Kerns, E. H. *Drug–Like Properties: Concepts, Structure, Design, and Methods from ADME to Toxicity Optimization*, 2nd ed.; Academic Press: London, 2016; pp 339-350.
57. Fesce, R.; Fumagalli, G. Drug Distribution and Ellimination. In *General and Molecular Pharmacology: Principles of Drug Action*, 1st ed.; Clementi, F.; Fumagalli, G., Eds.; John Wiley & Sons: Hoboken, 2015; pp 45-60.

58. Rankovic, Z. CNS Drug Design: Balancing Physicochemical Properties for Optimal Brain Exposure. *J. Med. Chem.* **2015**, *58*, 2584-2608.

59. Van Dam, D.; De Deyn, P. P. Drug Discovery in Dementia: the Role of Rodent Models. *Nat. Rev. Drug Discovery* **2006**, *5*, 956-970.

60. Ebert, U.; Kirch, W. Scopolamine Model of Dementia: Electroencephalogram Findings and Cognitive Performance. *Eur. J. Clin. Invest.* **1998**, *28*, 944-949.

61. Bajo, R.; Pusil, S.; López, M. E.; Canuet, L.; Pereda, E.; Osipova, D.; Maestú, F.; Pekkonen, E. Scopolamine Effects on Functional Brain Connectivity: a Pharmacological Model of Alzheimer's Disease. *Sci. Rep.* **2015**, *5*, 9748.

62. Klinkenberg, I.; Blokland, A. The Validity of Scopolamine as a Pharmacological Model for Cognitive Impairment: a Review of Animal Behavioral studies. *Neurosci. Biobehav. Rev.* **2010**, *34*, 1307-1350.

63. Snyder, P. J.; Bednar, M. M.; Cromer, J. R.; Matuff, P. Reversal of Scopolamine-Induced Deficits with a Single dose of Donepezil, an Acetylcholinesterase Inhibitor. *Alzheimer's Dementia* **2005**, *1*, 126-135.

64. Bouger, P. C.; van der Staay F. J. Rats with Scopolamine- or MK-801-Induced Spatial Discrimination Deficits in the Cone Field Task: Animal Models for Impaired Spatial Orientation Performance. *Eur. Neuropsychopharmacol.* **2005**, *15*, 331-346.

65. van der Staay, F. J.; Bouger, P. C. Effects of the Cholinesterase Inhibitors Donepezil and Metrifonate on Scopolamine-Induced Impairments in the Spatial Cone Field Orientation Task in Rats. *Behav. Brain Res.* **2005**, *156*, 1-10.

66. Stemmelin, J.; Cassel, J. C.; Will, B.; Kelche, C. Sensitivity to Cholinergic Drug Treatments of Aged Rats with Variable Degrees of Spatial Memory Impairment. *Behav. Brain Res.* **1999**, *98*, 53-66.

67. Vardigan, J. D.; Cannon, C. E.; Puri, V.; Dancho, M.; Koser, A.; Wittmann, M.; Kuduk, S. D.; Renger, J. J.; Uslaner, J. M. Improved Cognition Without Adverse Effects: Novel M1 Muscarinic Potentiator Compares Favorably to Donepezil and Xanomeline in Rhesus Monkey. *Psychopharmacology (Berl).* **2015**, *232*, 1859-1866.

68. Patil, S. S.; Sunyer, B.; Höger, H.; Lubec, G. Evaluation of Spatial Memory of C57BL/6J and CD1 Mice in the Barnes Maze, the Multiple T-Maze and in the Morris Water Maze. *Behav. Brain Res.* **2009**, *198*, 58-68.

69. Puzzo, D.; Lee, L.; Palmeri, A.; Calabrese, G.; Arancio, O. Behavioral Assays with Mouse Models of Alzheimer's Disease: Practical Considerations and Guidelines. *Biochem. Pharmacol.* **2014**, *88*, 450-467.

70. Vorhees, C. V.; Williams, M. T. Morris Water Maze: Procedures for Assessing Spatial and Related Forms of Learning and Memory. *Nat. Protoc.* **2006**, *1*, 848-858.

71. Knez, D.; Brus, B.; Coquelle, N.; Sosič, I.; Šink, R.; Brazzolotto, X.; Mravljak, J.; Colletier J. P.; Gobec, S. Structure-Based Development of Nitroxoline Derivatives as Potential Multifunctional Anti-Alzheimer Agents. *Bioorg. Med. Chem.* **2015**, *23*, 4442-4452.

72. Brazzolotto, X.; Wandhammer, M.; Ronco, C.; Trovaslet, M.; Jean, L.; Lockridge, O.; Renard, P. Y.; Nachon, F., Human Butyrylcholinesterase Produced in Insect Cells: Huprine-Based Affinity Purification and Crystal Structure. *FEBS J.* **2012**, *279*, 2905-2916.

73. Kabsch, W., Xds. *Acta Crystallogr., Sect. D: Biol. Crystallogr.* **2010**, *66*, 125-132.

74. McCoy, A. J.; Grosse-Kunstleve, R. W.; Adams, P. D.; Winn, M. D.; Storoni, L. C.; Read, R. J., Phaser Crystallographic Software. *J. Appl. Crystallogr.* **2007**, *40*, 658-674.

75. Adams, P. D.; Afonine, P. V.; Bunkoczi, G.; Chen, V. B.; Davis, I. W.; Echols, N.; Headd, J. J.; Hung, L. W.; Kapral, G. J.; Grosse-Kunstleve, R. W.; McCoy, A. J.; Moriarty, N. W.; Oeffner, R.; Read, R. J.; Richardson, D. C.; Richardson, J. S.; Terwilliger, T. C.; Zwart, P. H.

Phenix: A Comprehensive Python-Based System for Macromolecular Structure Solution. *Acta Crystallogr., Sect. D: Biol. Crystallogr.* **2010**, *66*, 213-221.

76. Emsley, P.; Lohkamp, B.; Scott, W. G.; Cowtan, K., Features and Development of Coot. *Acta Crystallogr., Sect. D: Biol. Crystallogr.* **2010**, *66*, 486-501.
77. Schuttelkopf, A. W.; van Aalten, D. M., Prodrg: A Tool for High-Throughput Crystallography of Protein-Ligand Complexes. *Acta Crystallogr., Sect. D: Biol. Crystallogr.* **2004**, *60*, 1355-1363.
78. Paxinos, G.; Watson, C. *The Rat Brain in Stereotaxic Coordinates 7nd ed*; Academic Press: San Diego, 2007.
79. Žakelj, S.; Berginc, K.; Roškar, R.; Kraljič, B.; Kristl, A. Do the Recommended Standards for in Vitro Biopharmaceutic Classification of Drug Permeability Meet the "Passive Transport" Criterion for Biowaivers? *Curr. Drug. Metab.* **2013**, *14*, 21-27.
80. Banker, M. J.; Clark, T. H.; Williams, J. A. Development and Validation of a 96-Well Equilibrium Dialysis Apparatus for Measuring Plasma Protein Binding. *J. Pharm. Sci.* **2003**, *92*, 967-974.
81. Di, L.; Kerns, E. H.; Hong, Y.; Chen, H. Development and Application of High Throughput Plasma Stability Assay for Drug Discovery. *Int. J. Pharm.* **2005**, *297*, 110-119.
82. Obach, R. S.; Baxter, J. G.; Liston, T. E.; Silber, B. M.; Jones, B. C.; MacIntyre, F.; Rance, D. J.; Wastall P. The Prediction of Human Pharmacokinetic Parameters from Preclinical and in Vitro Metabolism Data. *J. Pharmacol. Exp. Ther.* **1997**, *283*, 46-58.
83. DiResta, G. R.; Lee, J.; Lau, N.; Ali, F.; Galicich, J. H., Arbit, E. Measurment of Brain Tissue Density Using Pycnometry. In *Brain Edema VIII*, 1st ed.; Reulen, H. J.; Baethmann, A.; Fenstermacher, J.; Marmarou, A.; Spatz, M., Eds.; Springer: Vienna, 1990; pp 34-36.

84. U.S. Department of Health and Human Services, Food and Drug Administration, Center for Drug Evaluation and Research (CDER), Center for Veterinary Medicine (CMV) Guidance for Industry, Bioanalytical Method Validation **2011**, 1-22.

85. Matuszewski, B. K.; Constanzer, M. L.; Chavez-Eng, C. M. Strategies for the Assessment of Matrix Effect in Quantitative Bioanalytical Methods Based on HPLC-MS/MS. *Anal Chem.* **2003**, *75*, 3019-3030.

86. Patil, S. S.; Sunyer, B.; Höger, H.; Lubec, G. Evaluation of Spatial Memory of C57BL/6J and CD1 Mice in the Barnes Maze, the Multiple T-Maze and in the Morris Water Maze. *Behav. Brain Res.* **2009**, *198*, 58-68.

87. Puzzo, D.; Lee, L.; Palmeri, A.; Calabrese, G.; Arancio, O. Behavioral Assays with Mouse Models of Alzheimer's Disease: Practical Considerations and Guidelines. *Biochem. Pharmacol.* **2014**, *88*, 450-467.

88. Bialuk, I.; Dobosz, K.; Potrzebowski, B.; Winnicka, M. M. CP55,940 Attenuates Spatial Memory Retrieval in Mice. *Pharmacol. Rep.* **2014**, *66*, 931-36.

89. Sałat, K.; Podkowa, A.; Kowalczyk, P.; Kulig, K.; Dziubina, A.; Filipek, B.; Librowski, T. Anticonvulsant Active Inhibitor of GABA Transporter Subtype 1, Tiagabine, with Activity in Mouse Models of Anxiety, Pain and Depression. *Pharmacol. Rep.* **2015**, *67*, 465-72.

For Table of Contents Only